NASA/TM-20250005209

Forced Response of Distortion-Tolerant Fan Blades in a Boundary-Layer Ingesting Tail-Cone Thruster

James B. Min, Milind A. Bakhle, and Austin J. Schemmel
Glenn Research Center, Cleveland, Ohio

May 2025

NASA STI Program Report Series

Since its founding, NASA has been dedicated to the advancement of aeronautics and space science. The NASA scientific and technical information (STI) program plays a key part in helping NASA maintain this important role.

The NASA STI program operates under the auspices of the Agency Chief Information Officer. It collects, organizes, provides for archiving, and disseminates NASA's STI. The NASA STI program provides access to the NTRS Registered and its public interface, the NASA Technical Reports Server, thus providing one of the largest collections of aeronautical and space science STI in the world. Results are published in both non-NASA channels and by NASA in the NASA STI Report Series, which includes the following report types:

- TECHNICAL PUBLICATION.
  Reports of completed research or a major significant phase of research that present the results of NASA programs and include extensive data or theoretical analysis. Includes compilations of significant scientific and technical data and information deemed to be of continuing reference value. NASA counterpart of peer-reviewed formal professional papers but has less stringent limitations on manuscript length and extent of graphic presentations.

- TECHNICAL MEMORANDUM.
  Scientific and technical findings that are preliminary or of specialized interest, e.g., quick release reports, working papers, and bibliographies that contain minimal annotation. Does not contain extensive analysis.

- CONTRACTOR REPORT.
  Scientific and technical findings by NASA-sponsored contractors and grantees.

- CONFERENCE PUBLICATION.
  Collected papers from scientific and technical conferences, symposia, seminars, or other meetings sponsored or cosponsored by NASA.

- SPECIAL PUBLICATION.
  Scientific, technical, or historical information from NASA programs, projects, and missions, often concerned with subjects having substantial public interest.

- TECHNICAL TRANSLATION.
  English-language translations of foreign scientific and technical material pertinent to NASA's mission.

Specialized services also include organizing and publishing research results, distributing specialized research announcements and feeds, providing information desk and personal search support, and enabling data exchange services.

For more information about the NASA STI program, see the following:

- Access the NASA STI program home page at http://www.sti.nasa.gov

NASA/TM-20250005209

Forced Response of Distortion-Tolerant Fan Blades in a Boundary-Layer Ingesting Tail-Cone Thruster

James B. Min, Milind A. Bakhle, and Austin J. Schemmel
Glenn Research Center, Cleveland, Ohio

National Aeronautics and
Space Administration

Glenn Research Center
Cleveland, Ohio 44135

May 2025

Acknowledgments

The authors appreciate the assistance provided by Dr. Gregory Heinlein at NASA Glenn Research Center, who conducted the computational fluid dynamics analysis of the TCT blade using TURBO code. The authors also gratefully acknowledge the support provided by the Aeronautics Research Mission Directorate's Advanced Air Transport Technology Project.

This work was sponsored by the Advanced Air Vehicles Program at the NASA Glenn Research Center.

Level of Review: This material has been technically reviewed by technical management.

This report is available in electronic form at https://www.sti.nasa.gov/ and https://ntrs.nasa.gov/

NASA STI Program/Mail Stop 050
NASA Langley Research Center
Hampton, VA 23681-2199

Forced Response of Distortion-Tolerant Fan Blades in a Boundary-Layer Ingesting Tail-Cone Thruster

James B. Min, Milind A. Bakhle, and Austin J. Schemmel
National Aeronautics and Space Administration
Glenn Research Center
Cleveland, Ohio 44135

Abstract

NASA's Novel Propulsion Airframe Integration (NPAI) initiative explores advanced concepts such as boundary-layer ingestion (BLI) to improve propulsion efficiency and reduce fuel consumption. As part of this effort, the Boundary-Layer Ingesting Tail-Cone System (BLITS) features a tail-cone thruster (TCT) that accelerates the slow-moving boundary-layer airflow along the fuselage and wings, reducing drag and enhancing overall efficiency. However, ingesting distorted boundary-layer flow introduces aeromechanical challenges, including elevated vibration levels and reduced fan stability margins. This study investigates the forced response behavior of distortion-tolerant fan (DTF) blades under these conditions using high-fidelity finite element modeling, with unsteady aerodynamic pressures mapped from CFD to structural meshes. The results show that although circumferential nonuniformities in inlet pressure and swirl influence dynamic stress levels that are relevant to high cycle fatigue (HCF), the fan blade configuration maintains acceptable safety margins under the current TCT BLI DTF design conditions. These findings validate the robustness of the distortion-tolerant design and offer insights to support future improvements in BLI fan blade durability and aeromechanical performance.

1.0 Introduction

NASA is actively investing in Electrified Aircraft Propulsion (EAP) research to enhance fuel efficiency, reduce emissions, and minimize noise in commercial transport aircraft. This effort is part of the Advanced Air Transportation Technologies Project portfolio, which explores innovative propulsion-airframe integrated solutions. Various promising concepts have been proposed, incorporating advanced technologies such as high-aspect-ratio wings, boundary-layer ingestion (BLI), and hybrid-electric powertrains.

The primary goal of this research is to identify viable EAP concepts for narrow-body aircraft and advance key enabling technologies. Among these concepts, the Single-Aisle Turboelectric Aircraft with Aft Boundary Layer (STARC–ABL) propulsor shown in Figure 1 stands out as a 3-MW partially turboelectric configuration. Based on a conventional tube-and-wing design, STARC–ABL features a motor-driven tail-cone thruster that utilizes BLI to improve aerodynamic efficiency. BLI leverages the slower moving boundary-layer air along the fuselage and wings, accelerating it through an electrically driven ducted fan at the tail. This process reduces drag and lowers the thrust required for flight.

NASA's Glenn Research Center has been analyzing the STARC–ABL concept, forecasting that BLI alone could reduce fuel burn by 8 to 10 percent (Ref. 1). This improvement presents opportunities to extend flight range, lower operational costs, and enhance fuel efficiency through additional airframe modifications. Moreover, the indirect benefits—such as reduced weight and optimized fuselage shapes—could further amplify efficiency gains. As part of its broader research efforts, NASA continues to investigate BLI and other advanced aircraft designs aimed at achieving significant improvements in fuel efficiency.

Figure 1.—Represenative total pressure contours on wing-body-duct tail-cone thruster configuration.

Boundary-layer airflow distortion ingested through an electrically driven ducted fan at the tail introduces additional aeromechanical vibrations and reduced stability margins on fan blades. NASA Glenn continues to explore integrated aerodynamic-propulsion concepts that enhance performance, efficiency, and fuel savings for annular-type BLI configurations (Ref. 2). To address these challenges, a high-efficiency BLI flow Distortion-Tolerant Fan (DTF) rotor system has been studied as part of the Novel Propulsion Airframe Integration (NPAI) Boundary-Layer Ingesting Tail-Cone System (BLITS) project. This initiative evaluates the efficiency and fuel burn benefits of tail-cone thruster propulsion systems that ingest viscous boundary layers and distorted flow.

BLI propulsion inherently introduces persistent and severe inlet distortion at most operating conditions, potentially leading to high dynamic stresses due to aeroelastic forced responses, as well as the risk of flutter. These aeromechanical phenomena can result in fan structural failure caused by high cycle fatigue (HCF) or unstable self-excited vibrations. Modeling this dynamically interconnected problem through numerical simulations presents a significant challenge. In particular, aeromechanical vibration stresses in fan blades due to airflow distortion are a key concern, as increased stress levels can lead to premature blade failure. The assessment of the vibration dynamics of BLI-distorted flow-tolerant fan blades is therefore critical for the feasibility of tail-cone thruster (TCT) engine concepts.

Turbomachinery blade vibration stress has historically been a major cause of engine development setbacks. Reports indicate that more than 90 percent of potential HCF issues are identified during the development testing of new engines, contributing to nearly 30 percent of total development costs (Ref. 3). Thus, a primary objective of this study is to conduct aeromechanics forced response analysis on the TCT BLI DTF fan rotor system.

Aeromechanics forced response analysis provides critical insights into fan blade behavior, allowing engineers to identify and mitigate potential issues before significant damage occurs. Early detection of vibration-related problems enables corrective actions to be taken well before costly engine failures arise. By incorporating the necessary design precautions to minimize blade vibrations, the likelihood of mechanical faults can be significantly reduced, ensuring the reliability and efficiency of future BLI propulsion systems.

Using cyclic symmetry finite element modeling (FEM) techniques, this analysis aims to quantify the dynamic stresses experienced by a TCT BLI DTF fan blade operating in a continually distorted flow environment. The results will help assess the potential for HCF-related issues due to forced response blade dynamic stresses.

2.0 Formulations for Modeling Approaches

Turbomachinery blade vibrations are governed by complex dynamic interactions among structural, aerodynamic, and inertial forces. These vibrations are typically classified as either forced responses, induced by external or periodic aerodynamic excitations, or self-excited instabilities, such as flutter.

One of our primary objectives was to develop a model capable of determining the natural frequencies and mode shapes that could lead to resonances across the entire engine operating range. This requires integrating formulations from structural dynamics, structural mechanics, and fluid dynamics. Additionally, structural vibrations and aerodynamic damping were incorporated to characterize aerodynamic and structural behaviors, as well as to assess the performance of a distortion-tolerant fan-rotor configuration.

A key focus of this study is the aeromechanical vibration stresses induced by circumferential nonuniformity of inlet pressure and swirl as airflow enters the fan. The fluid dynamics of the airframe and propulsor inlet generate excitation forces, with frequencies dependent on the engine's rotational speed. When this excitation frequency matches the natural frequency of the fan blades, high vibration amplitudes can occur, potentially leading to HCF failure.

Traditional single-blade modeling techniques are inadequate for accurately capturing the dynamic loading behaviors and vibrational characteristics of an entire rotor system operating in distorted flow conditions. Therefore, an advanced modeling approach is necessary to account for these complexities. Figure 2 presents a flowchart outlining the framework of the current computational procedures, which

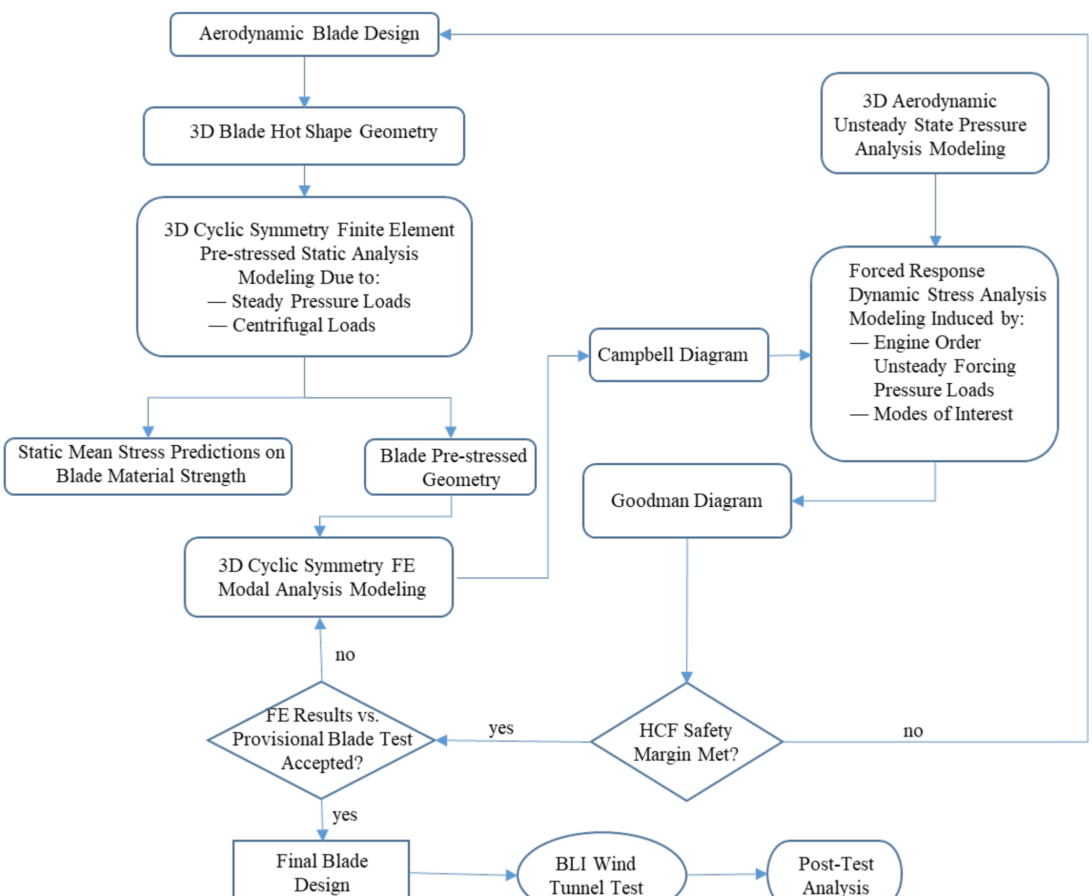

Figure 2.—Framework components of current computational procedures.

are evolving to support the development of aeromechanics design analysis models. In this context, the term "formulation" refers to the integration of computational methods that enable the solution of the forced response problem by coupling CFD-derived aerodynamic loads with structural finite element (FE) models. This coupling is a foundational step in building a fluid-structure interaction (FSI) analysis capability, which is essential for accurately capturing the dynamic interaction between aerodynamic forces and structural vibrations in a distortion-tolerant fan-rotor system.

2.1 Cyclic Symmetry Structural FEM Method

A key objective of this study is to develop a high-fidelity, full-rotor analysis capability for predicting the forced response of a TCT BLI fan blade system subjected to distorted flow. This was achieved using a cyclic symmetry FEM method (Ref. 4). This model reduction technique enables computationally efficient analysis by considering only a small periodic sector of the full TCT fan rotor blade system. It also allows for the incorporation of traveling wave excitations due to unsteady distorted flow in the circumferential direction of the rotor. Although this approach expedites forced response analysis of TCT engine fan blades and reduces dependence on wind tunnel testing, the computational results still require validation against experimental data to ensure accuracy. Traditional single-blade analysis models, widely used in turbomachinery research, are inadequate for capturing both the harmonic modal behavior and the forced response of blades subjected to complex distorted flow dynamics and vibrations.

A complete 360° rotor blade model would provide the most accurate representation of the mechanical and aerodynamic interactions within a turbomachinery system. However, full-rotor modeling is computationally expensive and impractical for large turbomachinery rotors exhibiting geometric nonaxisymmetry (nonaxisymmetric in structure, though not necessarily in aerodynamic performance). To address this challenge, model reduction techniques are essential. The cyclic symmetry modeling method was implemented in conjunction with TURBO, an implicit finite-volume aerodynamic analysis code that utilizes structured multiblock grids for fan flow modeling (Refs. 5 and 6). The ANSYS® (Ansys, Inc.) FE program was used to mesh the TCT BLI DTF rotor sector model with higher-order tetrahedral elements. Surface elements were generated on the blade surface to apply pressure loads.

In brief, the cyclic symmetry method enables the analysis of a fan-rotor system by solving only a single sector (the basic sector) while enforcing continuity and compatibility boundary conditions between cyclic substructures. This drastically reduces model size and computational cost (Refs. 7 to 9). By leveraging cyclic symmetry, the entire fan-rotor assembly can be represented using a single sector that includes the airfoil, platform, dovetail, and disk for inserted blades or a blisk (blade-integrated disk) sector if the blades and disk are integral parts of a single structure. This computationally efficient model accurately captures harmonic vibration modes and static stress distributions.

Following the cyclic symmetry vibration modal analysis, a cyclic symmetry harmonic forced response analysis was formulated to predict displacement amplitudes and dynamic stresses in the blades under given engine order (EO) unsteady aerodynamic pressure loads. These results were then used to assess the HCF durability of the TCT BLI DTF blade design.

This cost-effective cyclic symmetry finite element analysis (FEA) method enables a comprehensive study of the structural behavior of a rotating TCT BLI DTF bladed rotor system made from titanium material. Material properties for Ti-6Al-4V titanium, listed in Table I, were used for this analysis.

TABLE I.—TITANIUM TI-6AL-4V MATERIAL PROPERTIES

Young's Modulus	1.653e+7 psi
Poisson's Ratio	0.33
Density	0.16 lb_m/in^3
Tensile Yield Strength	159,542 psi
Compressive Yield Strength	155,190 psi

2.2 Sector Model Blade Geometry and Applied Boundary Conditions

Figure 3 illustrates the sector model geometry of the TCT BLI DTF rotor system along with the applied boundary conditions for the assessment. The geometric dimension from the inner radius of the disk to the blade tip is approximately 5.5 in. along the X-axis, as shown in Figure 3.

The thicker portion of the disk spans approximately 2.2 in. in the circumferential Y-direction, while the axial length of the rotor in the Z-direction is approximately 3.0 in. Sixteen blades were placed symmetrically around the disk, so a 22.5° sector was used to produce a symmetric sector. The size of this scale-model fan is designed to match a planned wind tunnel test. In actual application, the fan would be significantly larger but rotate at a much slower speed.

2.3 FE Meshing With Higher Order Tetrahedral Elements

Figure 4 and Figure 5 illustrate the quality and density of the FE meshes, with particular attention given to regions where high stresses are likely to occur (Ref. 10). This approach ensures accurate stress prediction. The mesh quality is considered excellent for computational accuracy based on the aspect ratio of FE mesh and prior experience, though the large model size poses challenges for performing multiple forced response computations, even with the computationally efficient mode summation method (Ref. 11).

2.4 Aerodynamic Steady Pressure Loads From CFD Predictions Interpolated Onto Structural FE Meshes at Design Speed

Because the CFD grid and FEA structural mesh are not the same, a pressure mapping procedure is needed to interpolate pressure data for FSI in the aeromechanical forced response analysis. The steady and unsteady pressure field computed via CFD was interpolated onto the structural FE mesh using the surface-based projection technique with the ANSYS® program.

A time-domain unsteady Reynolds-averaged Navier-Stokes (URANS) solver, TURBO (Refs. 5 and 6), was used to model the unsteady flow field resulting from BLI distortion and fan blade vibrations. TURBO is an implicit finite-volume solver that employs structured multiblock grids for fan flow modeling.

Figure 6 presents the mean (steady-state) pressure contours mapped onto the FE mesh.

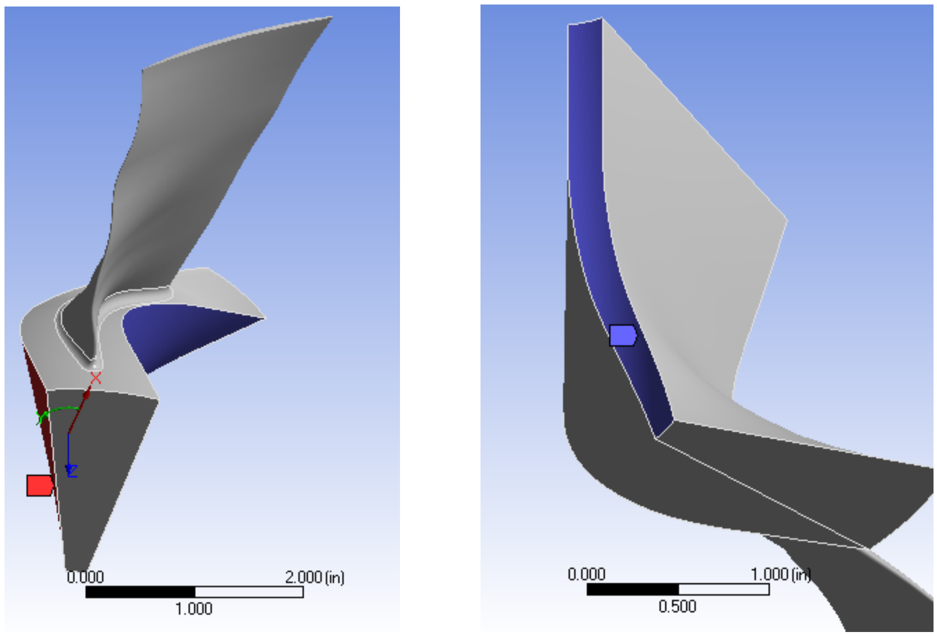

Figure 3.—Geometry of 22.5° sector for 16-blade TCT rotor: cyclic symmetry boundary conditions are shown on left (in blue) and fixed support boundary condition at inner radius is shown on right (in blue), along with coordinate system.

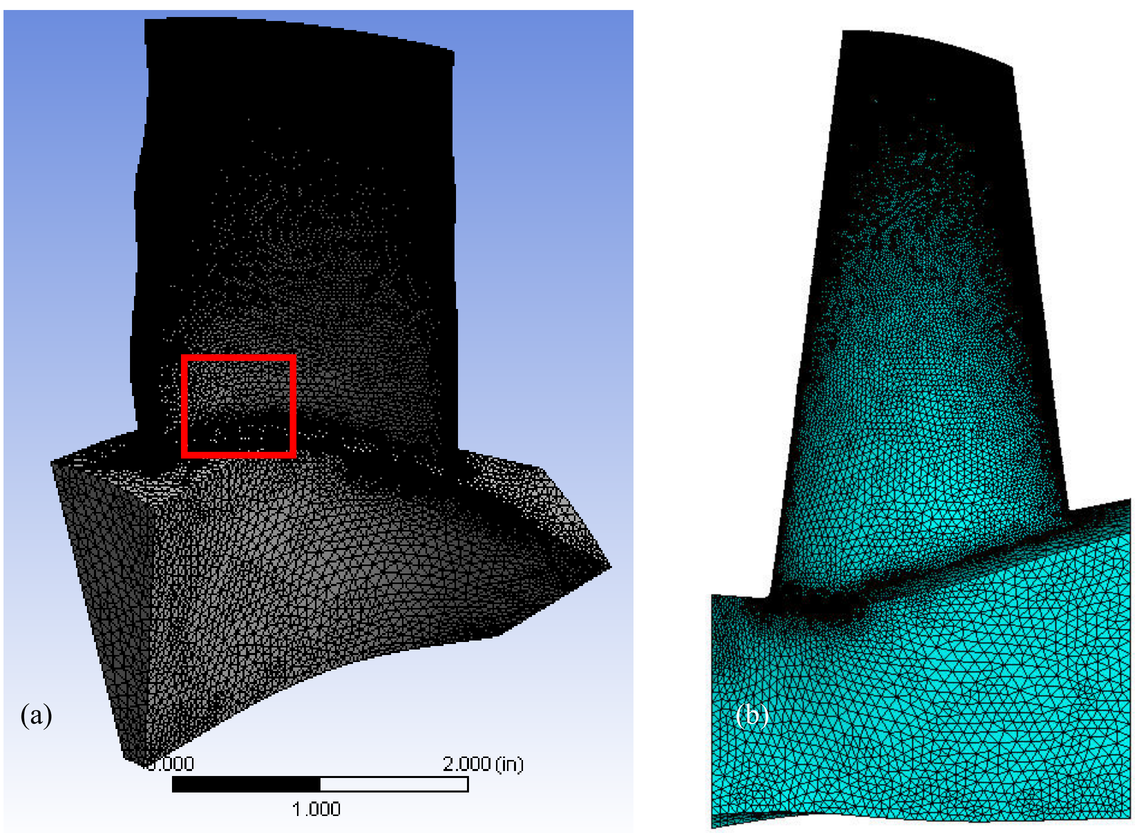

Figure 4.—FE meshed sector model used for analysis, comprising 1,834,259 elements and 2,383,369 nodes, with total of 7,150,107 degrees of freedom to be solved. (a) Isometric view. (b) Front view.

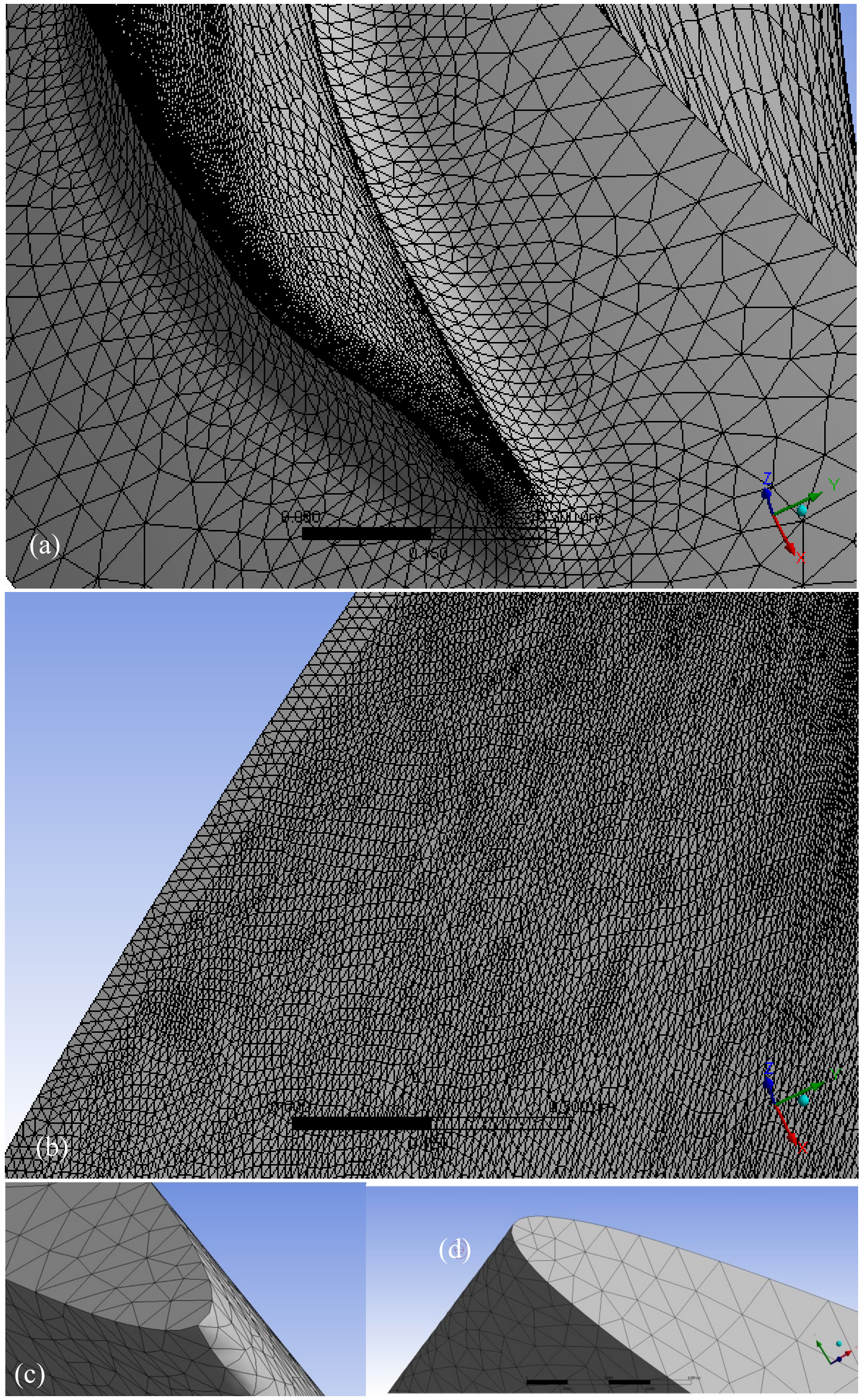

Figure 5.—Mesh quality close-ups. (a) Blade platform region, magnified view of area highlighted in red box in Figure 4(a). (b) Blade tip in thickness direction. (c) Trailing edge (d) Leading edge.

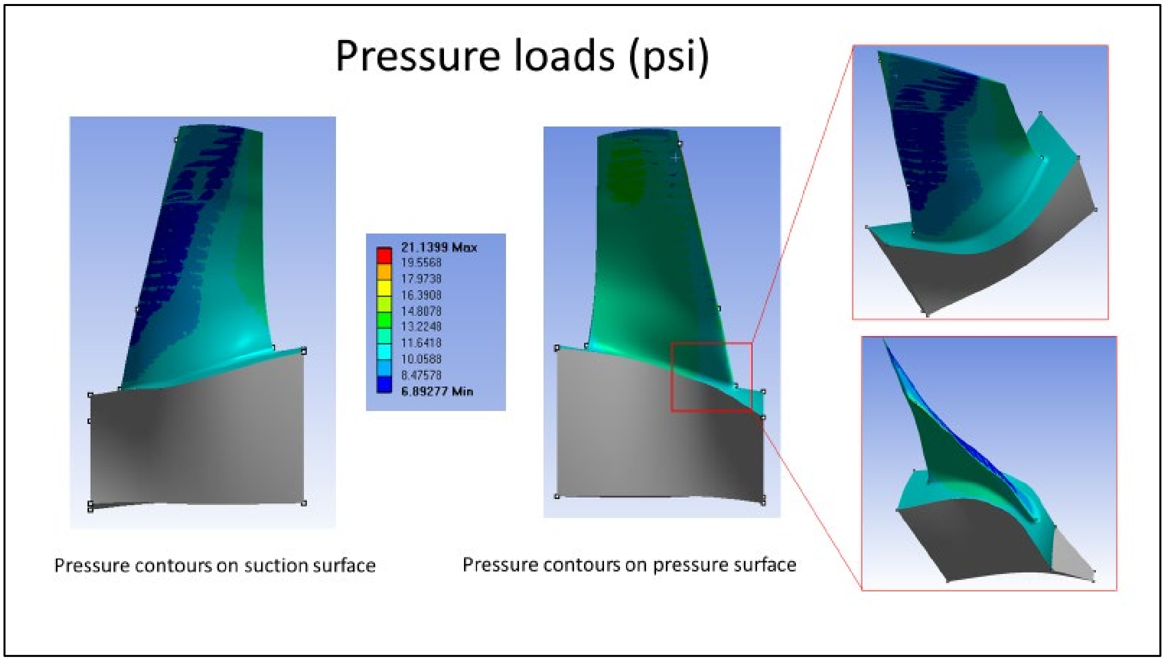

Figure 6.—Steady-state aerodynamic pressure contours mapped onto structural FE mesh from CFD analysis.

2.5 Static Stress Analysis From Aerodynamic Steady State Pressure and Fan Design Speed

The initial analysis focused on evaluating mean stresses under static conditions, incorporating nonlinear rotational effects such as spin softening and stress stiffening due to centrifugal loading from rotational velocity and steady-state aerodynamic blade pressure.

The TCT blade geometry analyzed was the design-intent operating blade shape rather than the as-manufactured blade geometry. Hence, small-deflection assumptions were applied in the analysis at 100 percent design speed (21,581 rpm) with corresponding steady-state aerodynamic pressure loads to assess mean stresses against the blade material strength data. Figure 7 presents the stress distribution resulting from rotational loading only, establishing a baseline for comparison. Figure 8 and Figure 9 incorporate both rotational and mean aerodynamic pressure loads, allowing the effects of steady-state pressure to be observed. The increase in maximum static stress from 119 to 123 ksi demonstrates how the inclusion of mean pressure loading influences the stress field. These effects are evident in the stress contours, providing insight into how aerodynamic pressure contributes to the overall structural response of the blade under design conditions. The static displacements presented are calculated from the hot shape geometry, which represents the design-intent operating blade shape. These displacements reflect the blade’s expected behavior once it reaches its operating temperature and steady-state conditions, under the aerodynamic loads predicted by the CFD analysis. This approach ensures that we understand how the blade will deform in its final, functional state, rather than its behavior from an as-manufactured, nonoperating shape. The displacements referred to are the computed deformation contours and amplitude values obtained under design speed loading conditions. These displacement results help assess the blade’s structural performance by identifying regions of high deflection, potential stress concentration, and dynamic behavior under operational conditions. Although experimental validation data are not currently available, the displacement patterns and magnitudes serve as a preliminary indicator for evaluating whether the structural response aligns with the expected behavior based on design assumptions, such as material linearity, boundary conditions, and loading.

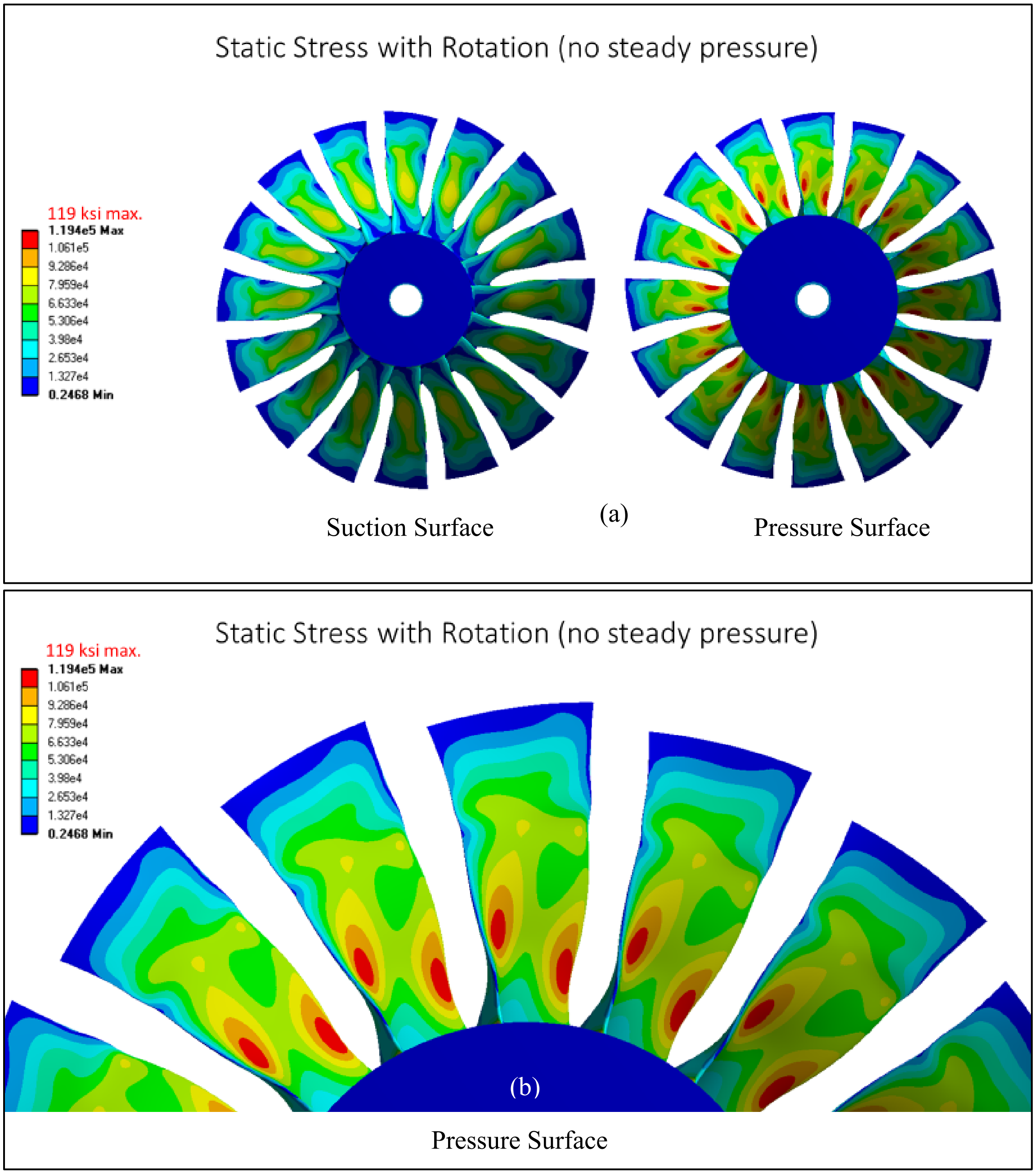

Figure 7.—Von Mises static stress contours on full rotor with rotation only, without aerodynamic steady-state pressure. (a) Global view. (b) Detailed view.

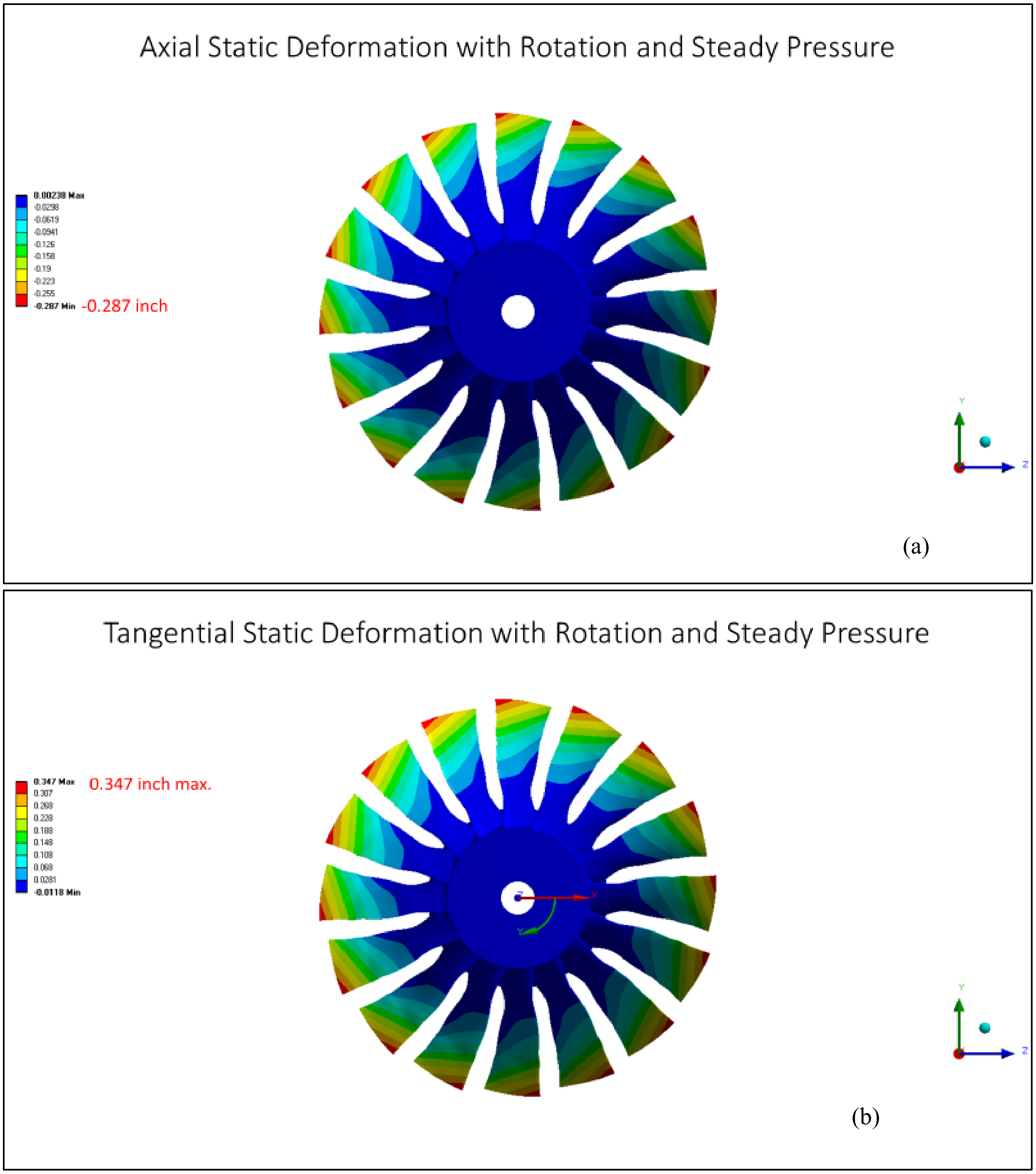

Figure 8.—Displacement contours. Single-sector model highlights clearer contours on blade surfaces under rotational and steady-state aerodynamic loads. (a) Axial direction. (b) Tangential (or circumferential) direction. (c) Radial direction. (d) Vector-sum displacement value. (e) Maximum displacement value.

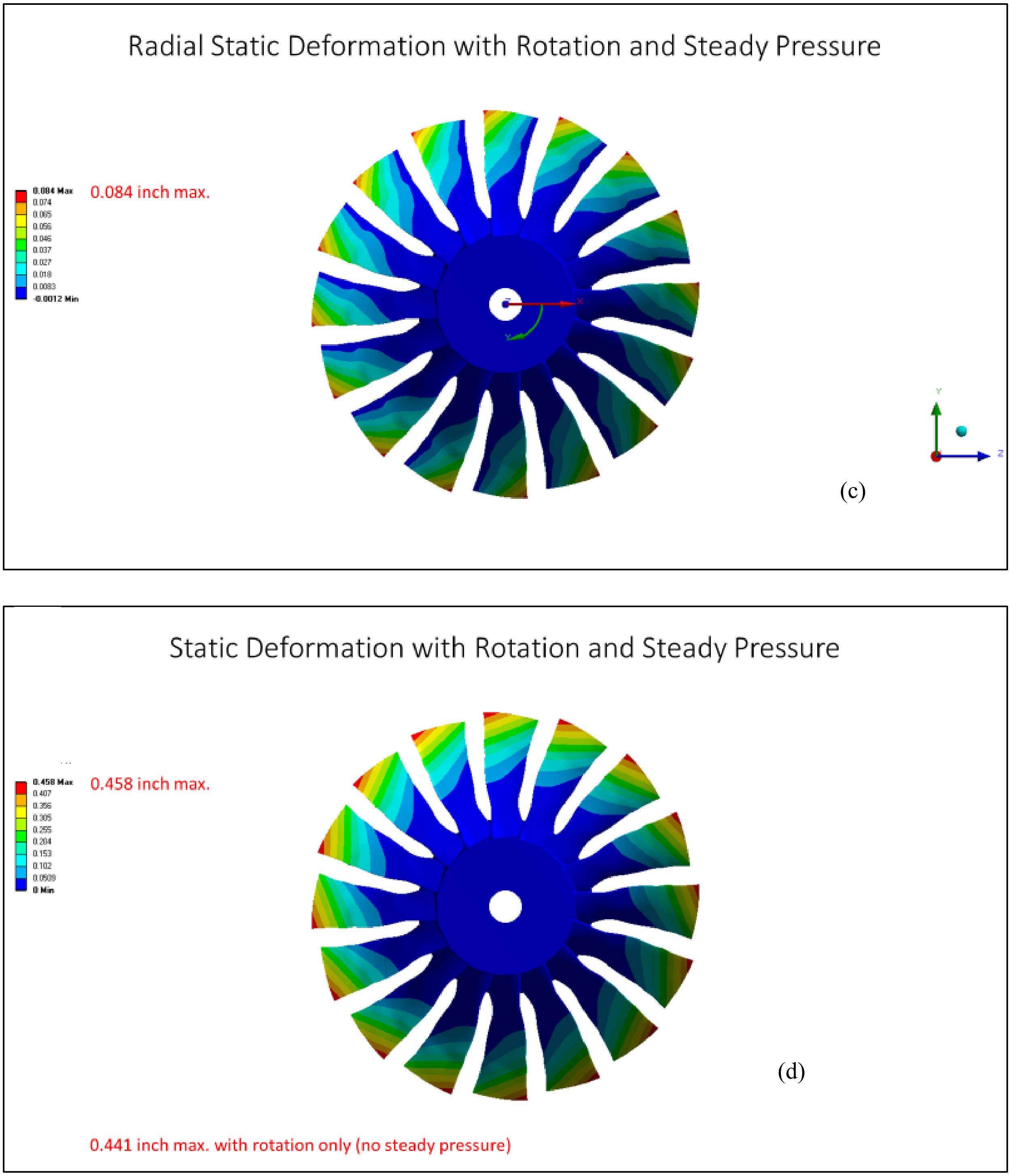

Figure 8.—Continued.

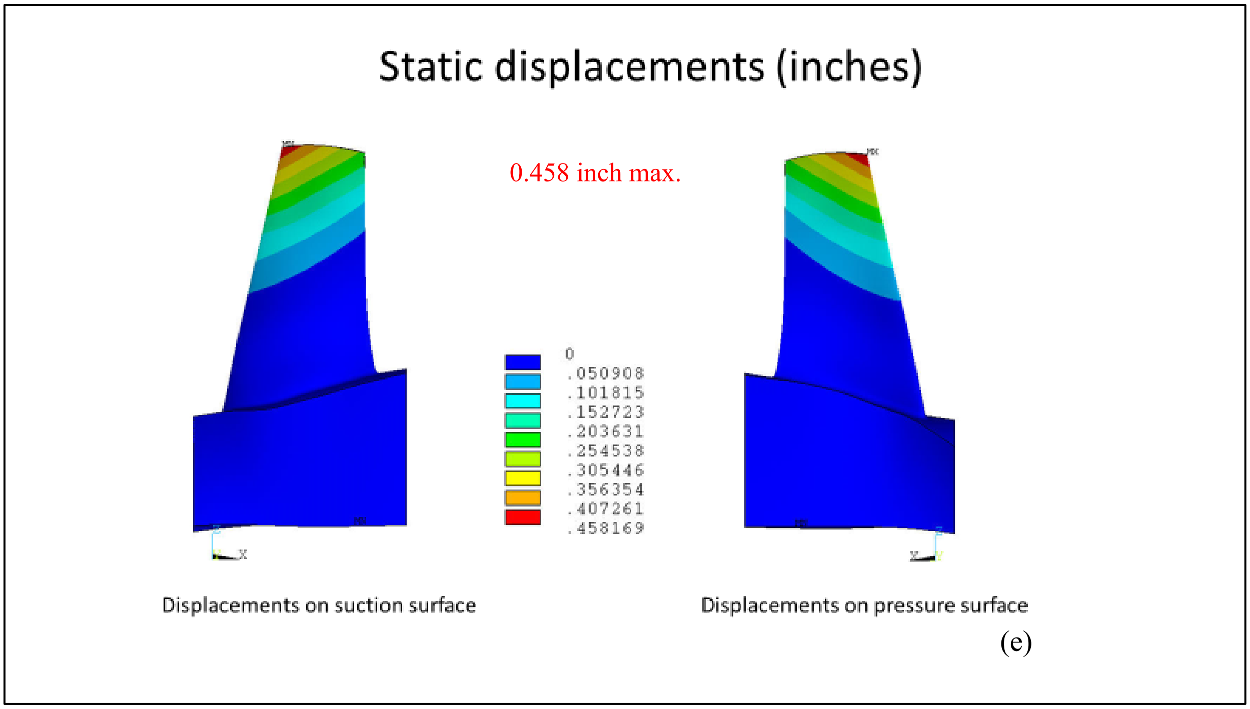

Figure 8.—Concluded.

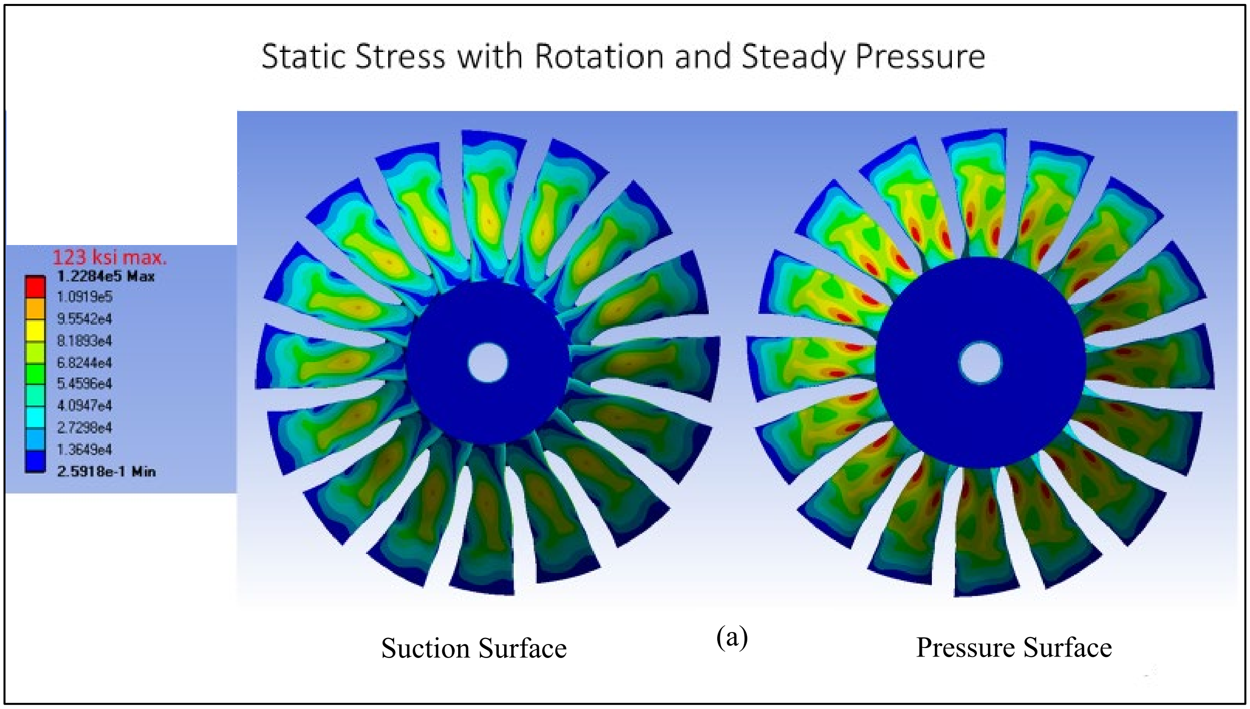

Figure 9.—Stress contours. Single-sector model shows clearer stress patterns under rotational and steady-state aerodynamic loads. (a) On full rotor surfaces. (b) Close-up view. (c) Maximum stress values.

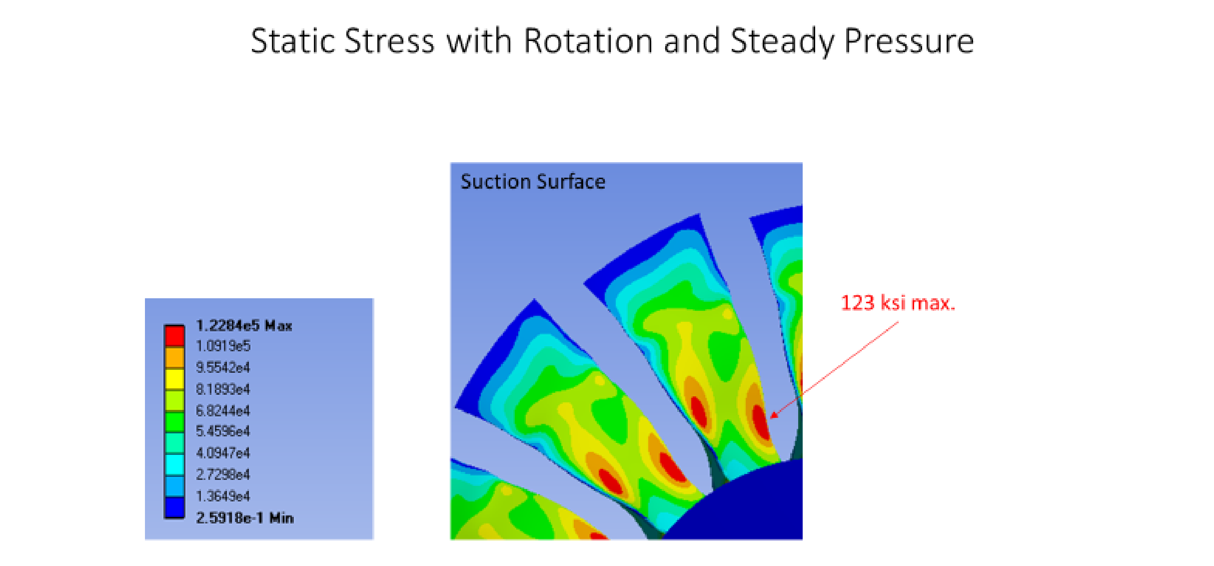

(b)

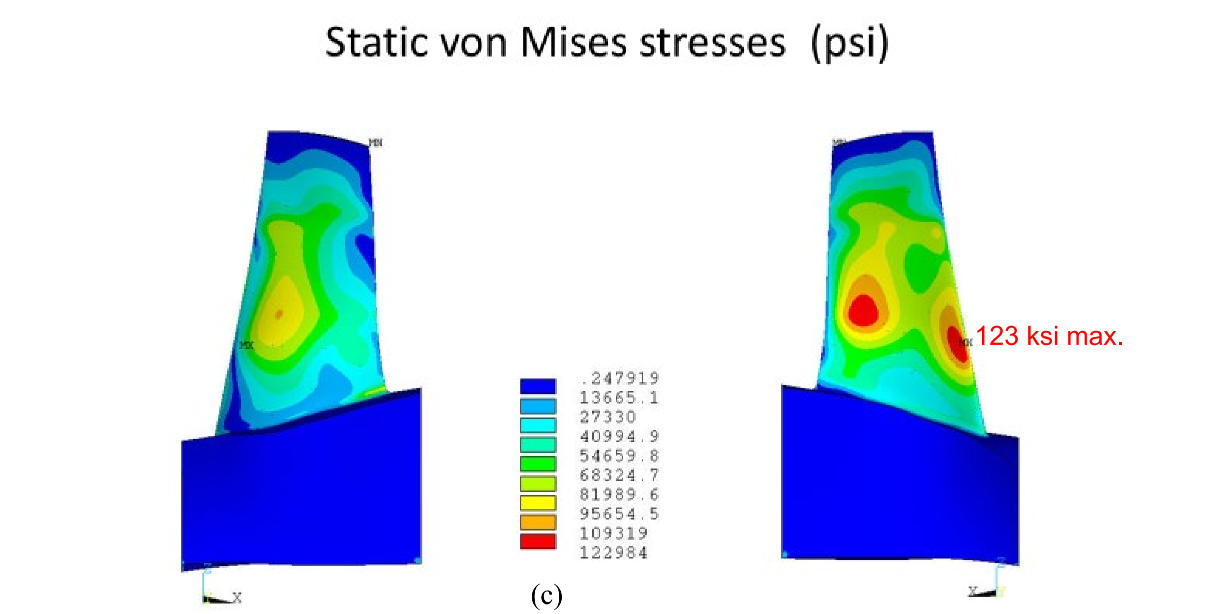

(c)

Figure 9.—Concluded.

2.6 Prestressed Cyclic Symmetry Modal Analysis and Results Under Aerodynamic Steady-State Pressure at Fan Design Speed

A rotating fan blade exhibits greater stiffness than a stationary blade due to the stiffening effect induced by centrifugal forces. A prestressed analysis was conducted by first performing a static analysis before the vibration modal analysis to account for the stresses and displacements influenced by centrifugal forces and aerodynamic steady-state pressure loads. A cyclic symmetry FE prestressed vibration modal analysis model was developed to simulate various fan operational conditions, ranging from 0 percent engine speed to an extended 140 percent engine speed, covering a wide range of speed conditions combined with aerodynamic effects, as described in Section 2.4. Note however that the aerodynamic pressure loads are not updated at the off-design speed analyses. This is justified based on the expected relatively small effect of the mean (steady-state) pressure loading on the natural frequencies calculated in the modal analysis.

This groundwork established the computational procedures necessary to understand the structural characteristics of the TCT blade configuration. Subsequently, a cyclic symmetry prestressed modal analysis was performed to extract natural frequency, modal displacement (mode shape), and modal stress data for the TCT fan blade in terms of nodal diameter (ND) information, considering both fan speeds and aerodynamic pressure effects.

In cyclic symmetry modal analysis, the theoretical concepts of harmonic indices and NDs were applied. At corresponding points in each blade sector, the vibration mode shapes exhibit sinusoidal patterns in the circumferential direction, forming nodal lines across the bladed disk system, known as nodal diameters (NDs). Most mode shapes include lines of zero out-of-plane displacement extending across the entire disk. The computed frequencies and mode shapes for the first three modes at one ND (ND1 or 1ND) are presented in Figure 10 and Figure 11.

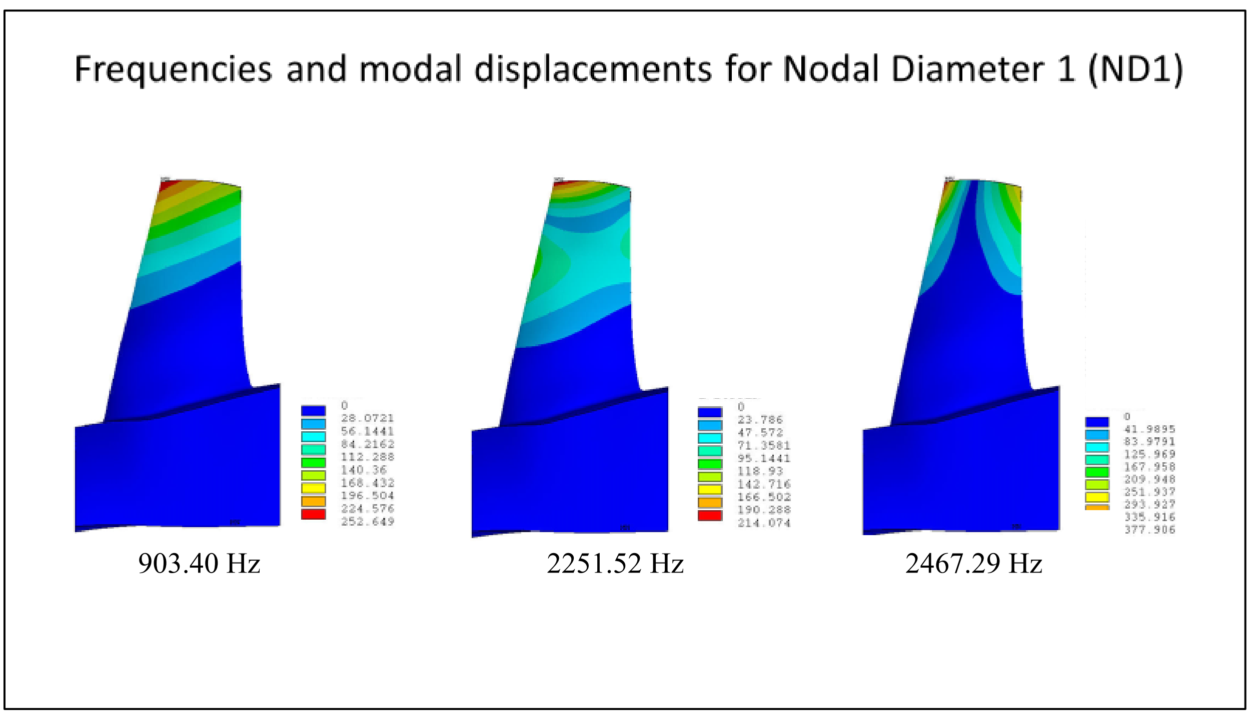

Figure 10.—ND mode shapes for first ND (1ND) of first three modes (mode 1, mode 2, and mode 3) in rotor sector model.

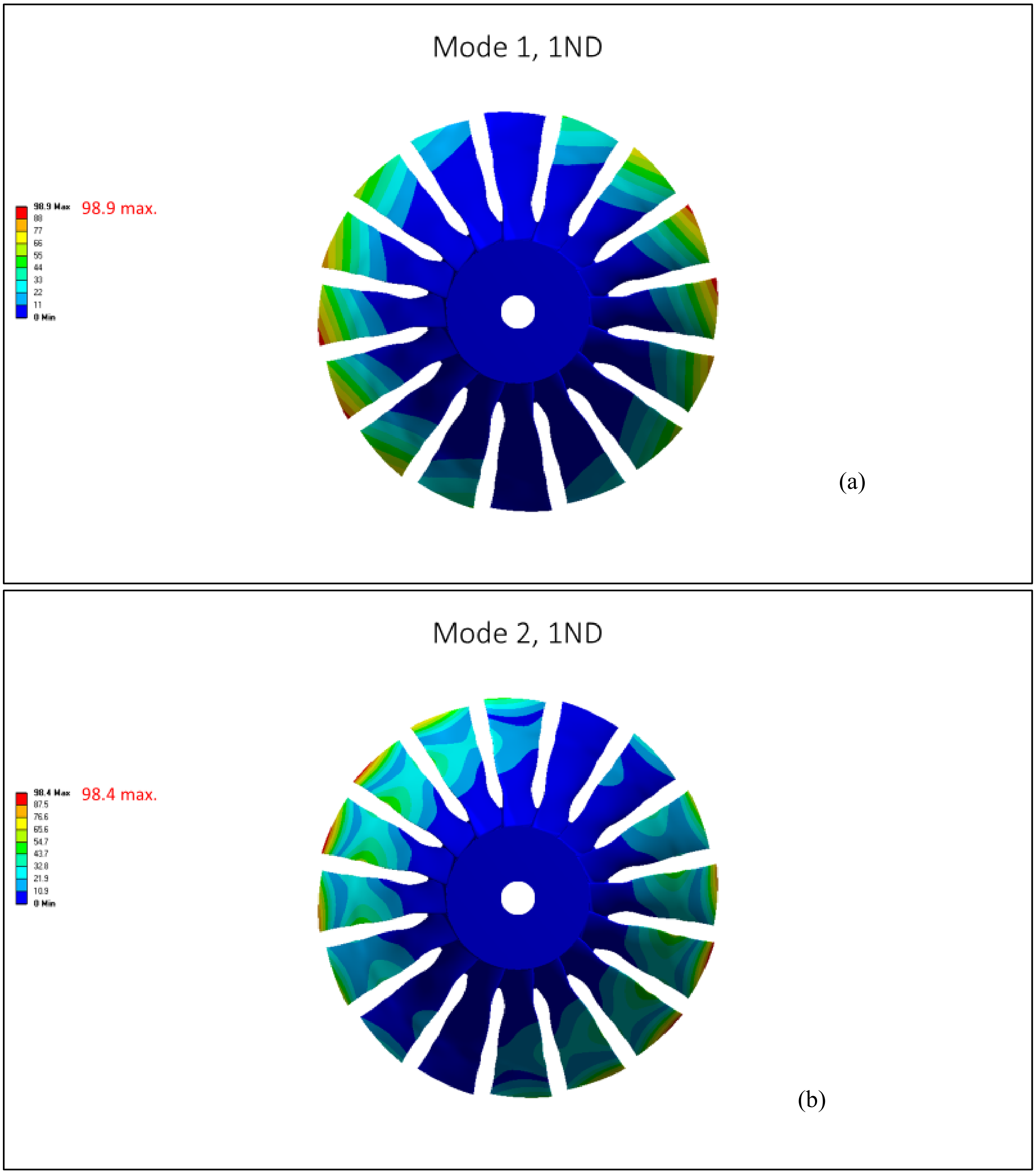

Figure 11.—ND mode shapes for first ND (1ND) of first three modes in fully bladed rotor model. (a) Mode 1. (b) Mode 2. (c) Mode 3.

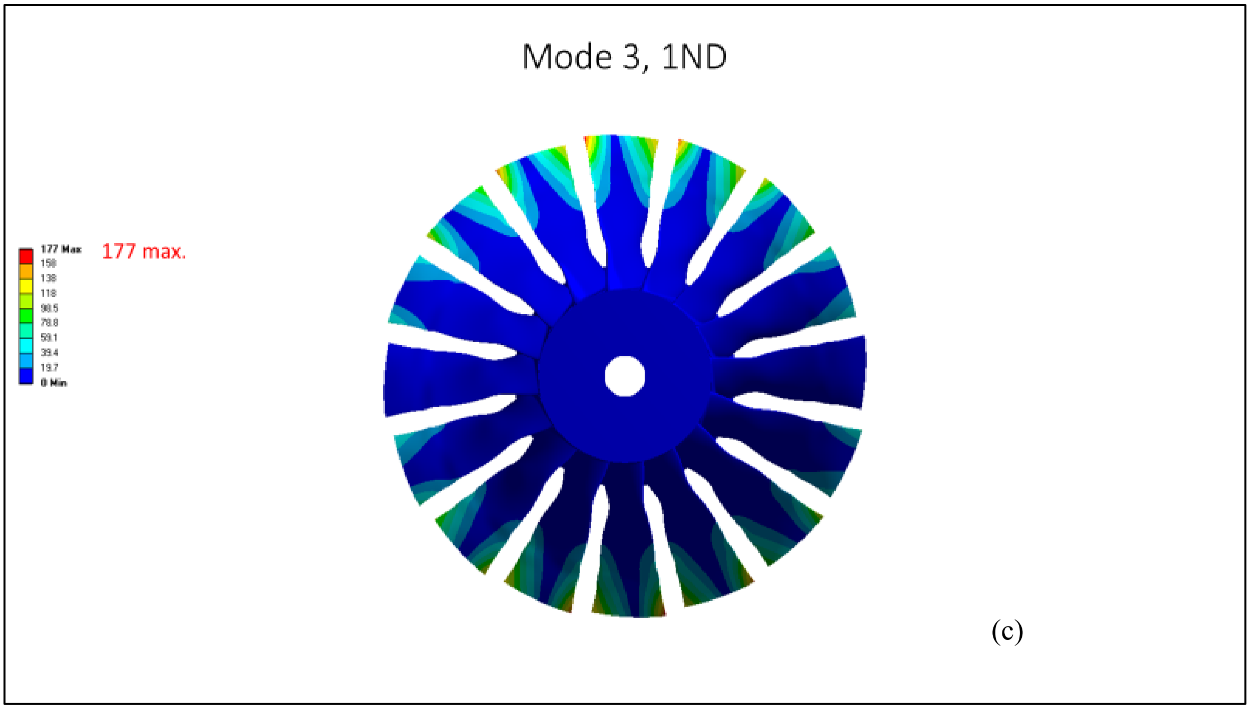

Figure 11.—Concluded.

2.7 Development of Campbell Diagram and Frequency Interference Evaluation Diagram

Subsequently, a prestressed cyclic symmetry vibration modal analysis was conducted to identify blade vibration frequencies and critical speed ranges. Several frequencies and mode shapes were calculated for a given set of TCT rotor NDs. The perturbed prestressed modal prediction method was employed, considering the creation of a perturbed prestressed mode superposition harmonic forced response analysis on the cyclic-sector model.

The first task was to develop a cyclic symmetry FE static analysis model that incorporates the TURBO steady-state aerodynamic blade pressure load as a function of fan blade rotation. To accurately capture the structural response of the blade under rotational conditions, geometric nonlinearity needed to be considered, as deflections can significantly alter the blade's geometry. Although solving the full nonlinear equilibrium equations iteratively provides the most precise prediction for large deformations, the computational cost for a model of this scale is prohibitively high. As an alternative, a small-deflection approach was adopted, with modifications to the structural stiffness matrix to approximate the effects of large deflections. This approach enables the model to account for dynamic mass effects while significantly reducing computational demands. In the present analysis, equilibrium conditions and centrifugal forces were formulated and solved within this adjusted small-deflection framework. As a result, the model includes the initial prestressed state from both linear and nonlinear static conditions. It is important to note that a rotating fan blade exhibits greater stiffness than a stationary one, due to centrifugal stiffening. This added stiffness is dependent on rotational speed, making the natural frequencies of the blade a function of rotation.

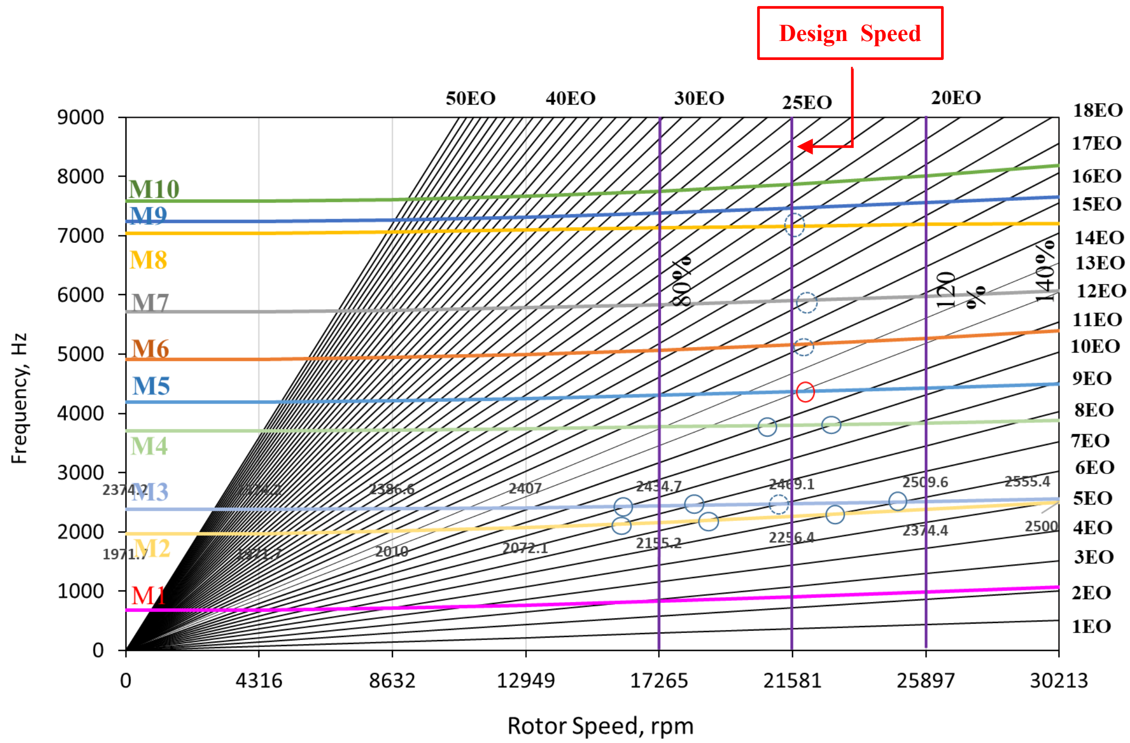

Figure 12.—Campbell diagram of TCT BLI DTF rotor, illustrating variation of natural frequencies with rotational speed, with potential EO crossings highlighted by circles.

TABLE II.—VARIATION OF MODAL FREQUENCIES WITH ROTOR SPEED

Hz \ rpm	0	4316	8632	12949	17265	21581	25897	30213
Mode 1	678.4	678.4	712.3	764.1	829.2	903.4	983.3	1066.5
Mode 2	1968.0	1968.0	2006.2	2068.0	2150.8	2251.5	2366.9	2493.9
Mode 3	2372.6	2372.6	2385.0	2405.3	2432.9	2467.3	2507.6	2553.3
Mode 4	3706.9	3706.9	3720.0	3740.9	3768.5	3801.3	3837.8	3876.1
Mode 5	4145.2	4145.2	4167.1	4202.0	4247.6	4301.5	4361.7	4426.5
Mode 6	4838.6	4838.6	4869.3	4920.2	4990.5	5078.9	5182.9	5298.7
Mode 7	5525.0	5525.0	5546.6	5581.9	5630.2	5690.4	5761.9	5844.2
Mode 8	6831.0	6831.0	6844.4	6865.0	6890.5	6918.3	6945.7	6969.6
Mode 9	7102.6	7102.6	7141.8	7203.0	7279.9	7365.8	7455.4	7546.1
Mode 10	7477.7	7477.7	7511.7	7570.5	7657.1	7773.2	7915.7	8056.9

These frequencies are typically represented using a Campbell diagram along with lines of constant slope that represent EO excitation (denoted as EO in Figure 12). A Campbell diagram allows a quick identification of speeds where the EO excitation lines intersect the natural frequency lines, indicating resonant conditions that can lead to large blade vibration response. The Campbell diagram in Figure 12 was developed and extended to 140 percent of the TCT BLI DTF design speed to further evaluate the structural characteristics across a broader range of off-design speeds. The solid colored lines represent the FEA-predicted modal resonance frequencies. The diagonal lines indicate EO excitation frequencies (e.g., 1EO, 2EO, etc.), while the vertical lines correspond to selected rotor speeds of interest, with percentages denoting fractions of the design speed. The following observations were made from the Campbell diagram. The natural frequencies of the first ten modes generally exhibit noticeable variation with increasing rotational speed, indicating a centrifugal stiffening effect in this blade design. However, this effect is relatively limited in certain modes—specifically modes 3, 4, and 8—as also shown in Table II. The primary characteristics of these mode shapes remains largely unaffected by the rotational speed. The mode shapes remain largely unchanged with varying rotational speed, even though their corresponding frequencies may shift noticeably.

For the first three critical modes, no resonance was observed at the design speed of 21,581 rpm. However, due to reliability and safety concerns regarding the TCT rotor blade design, a further assessment was conducted to better understand the effects of different ND characteristics and EO excitations. This assessment aimed to ensure that critical speeds—where excitation frequencies coincide with the structure's natural frequencies—would not occur in the current rotor blade design. Because such crossings cannot be eliminated, the focus is on avoiding crossings of lower order modes near the design speed where the fan would be expected to operate for extended duration.

In a rotor blade assembly, where multiple blades are connected by a disk, additional natural frequencies and more complex modes are present. This is because the blades behave as a coupled system, with interactions through the disk. The frequencies and modes depend on the number of blades and the blade-disk interaction behaviors. To further investigate possible critical speed crossings in the TCT rotor blade system, an interference diagram (Figure 13) was developed.

This diagram serves as a complementary tool to the Campbell diagram, offering more detailed insights into potential resonance frequencies. Furthermore, this diagram enables comparison not only of the EO harmonic excitation frequencies with the fan blade natural frequencies but also the shape of these harmonics in terms of the nodal mode shapes of a full 360° bladed rotor system, described by NDs. Note that a particular ND mode is excited only by the corresponding EO or an alias of a larger EO as denoted by the symbols in Figure 13. For example, ND4 mode can be excited by 4EO, 12EO, or 20EO with the actual level of response depending on the ratio of exciting and natural frequencies. This diagram helps identify which interference is likely to cause larger blade vibrations and resonances, thereby helping to avoid dangerous engine blade operation.

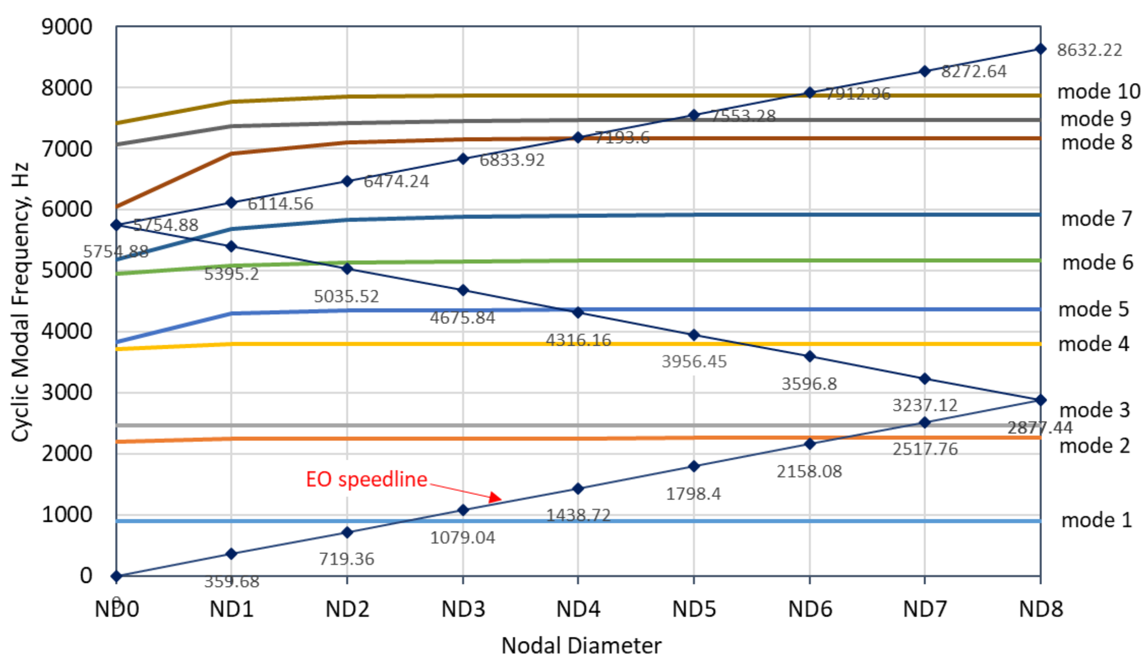

Figure 13.—Interference diagram at design speed.

3.0 Forced Response Analysis and Results

A FE forced response analysis method, utilizing the computationally efficient cyclic symmetry modeling approach (Refs. 4, 7 to 9), enabled a comprehensive study of various structural characteristics of the rotating TCT BLI DTF fan blade system. Modes and NDs of interest (Figure 14), identified from the Campbell diagram (Figure 12) and the interference diagram (Figure 13), were analyzed due to the small frequency margin associated with potential EO crossings.

Because the TCT fan rotor is assumed to be a blisk, the total damping is expected to come primarily from aerodynamic sources. The blisk's single-piece construction eliminates traditional mechanical joints—such as blade root connections—that often contribute to higher structural damping through frictional energy dissipation. Although this design offers advantages in strength and weight reduction, it also results in lower inherent vibration damping.

In the absence of specific aerodynamic damping data for this analysis, a total damping ratio of 0.03 percent was applied throughout the analysis. This value represents a combined estimate, accounting for both the low intrinsic material damping of the Ti-6Al-4V alloy and a baseline aerodynamic damping contribution. However, the actual total damping could be higher than the assumed 0.03 percent, especially without flow separation or flutter-prone modes. The use of 0.03 percent as the total damping ratio is thus considered a conservative assumption. It ensures that the forced response is not underestimated, while still acknowledging the potential stabilizing effect of positive aerodynamic damping. If more accurate aerodynamic damping data were available—such as from high-fidelity CFD-based aerodynamic damping predictions or experimental measurements—a higher total damping value might be justified, resulting in reduced predicted vibration amplitudes.

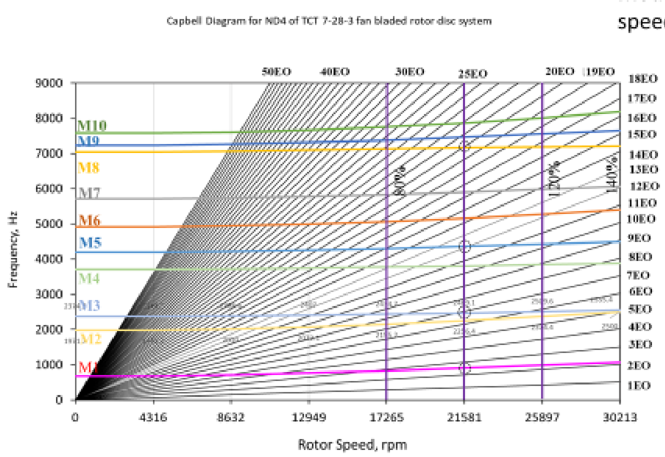

Modes and nodal diameters of interest at engine design speed (21581 rpm), identified from Campbell diagram

MODE	ND	EO
1	1	1
1	2	2
1	3	3
3	7	7
5	4	12
8	4	20

Figure 14.—Identified modes and NDs of interest from Campbell diagram.

The predicted unsteady flow field from a TURBO CFD analysis was used to extract a time history of pressure on the fan blades that was transformed to the frequency domain using a Fourier analysis to obtain EO excitations on the fan blades. Pressure contours on the fan blade, interpolated from the BLI distortion and blade vibrations, are shown in Figure 15 to Figure 20. As described in Figure 15, these interpolated unsteady pressure magnitudes and patterns—calculated from CFD analysis—are mapped onto the FE structural model mesh. These contours are presented in terms of EO harmonics for the forced response computations. EO excitation refers to the periodic forcing that arises from circumferential disturbances in a set of blades on the bladed rotor. Also, note that the complex-valued results of the Fourier analysis are represented here by the real and imaginary components for the forced response analysis to follow. These can also be represented as magnitude and phase if needed for better interpretation.

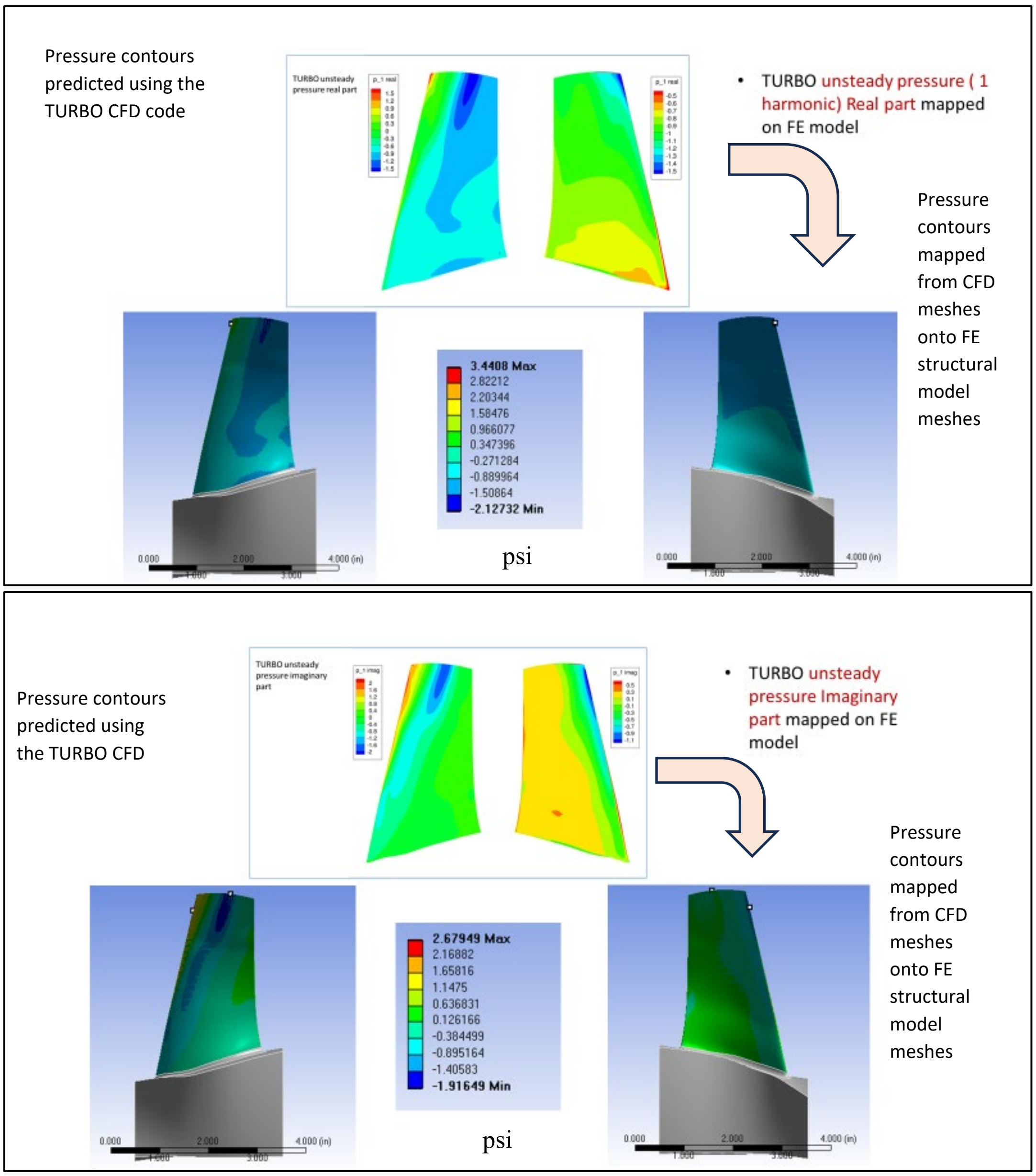

Figure 15.—Unsteady aerodynamic pressure contours (real and imaginary) for 1st EO harmonic excitation.

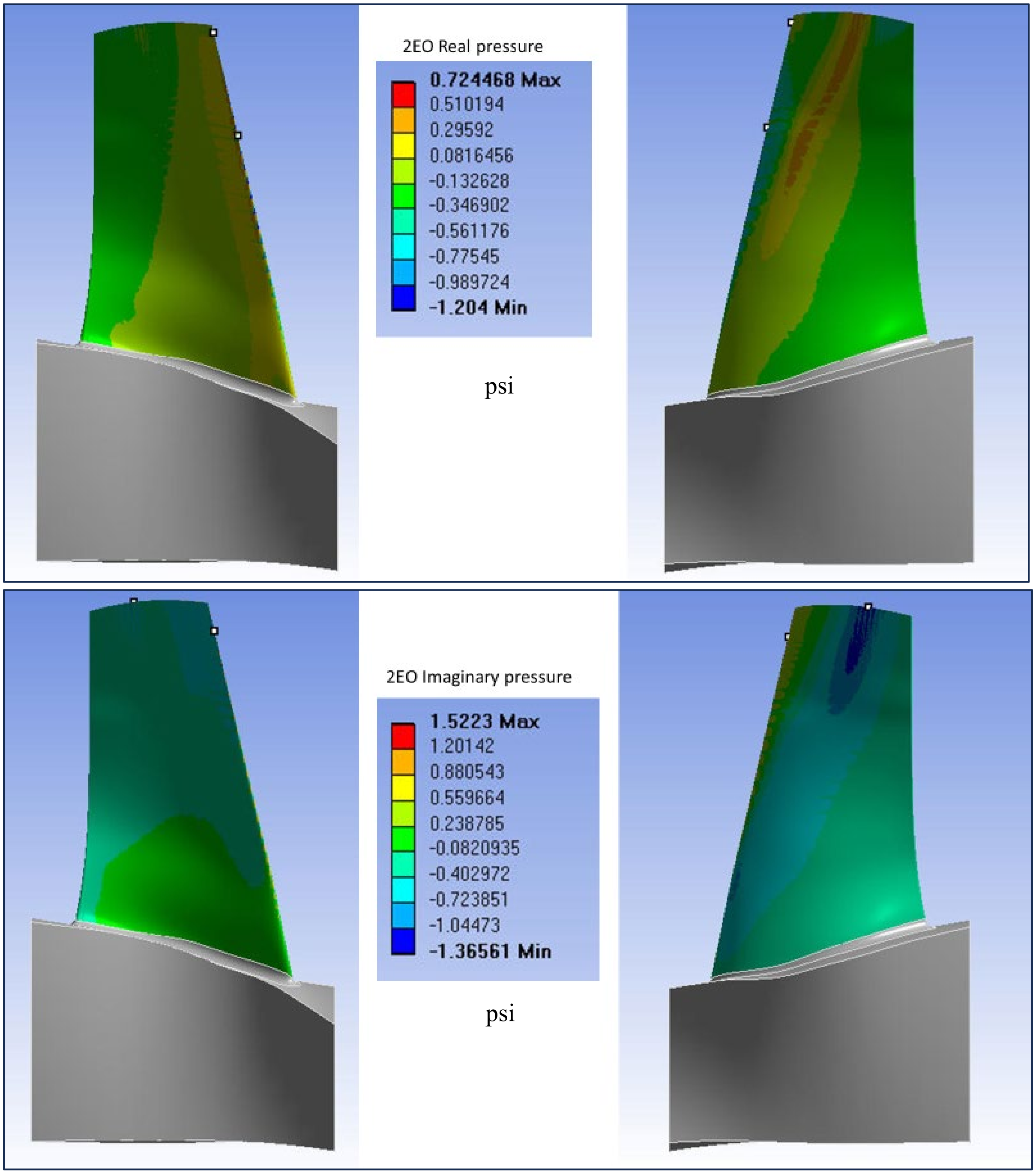

Figure 16.—Unsteady aerodynamic pressure contours (real and imaginary) for 2nd EO harmonic excitation.

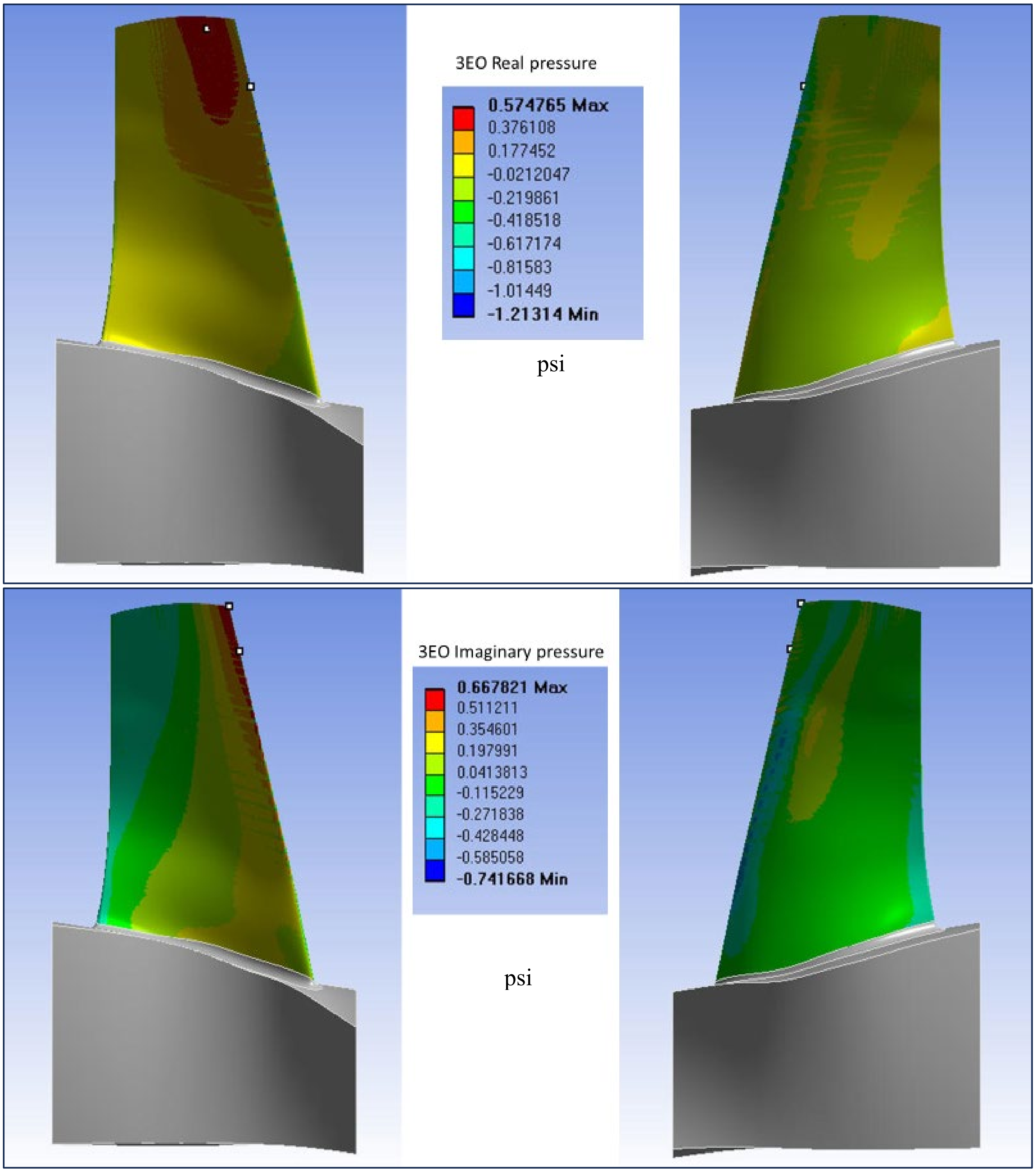

Figure 17.—Unsteady aerodynamic pressure contours (real and imaginary) for 3rd EO harmonic excitation.

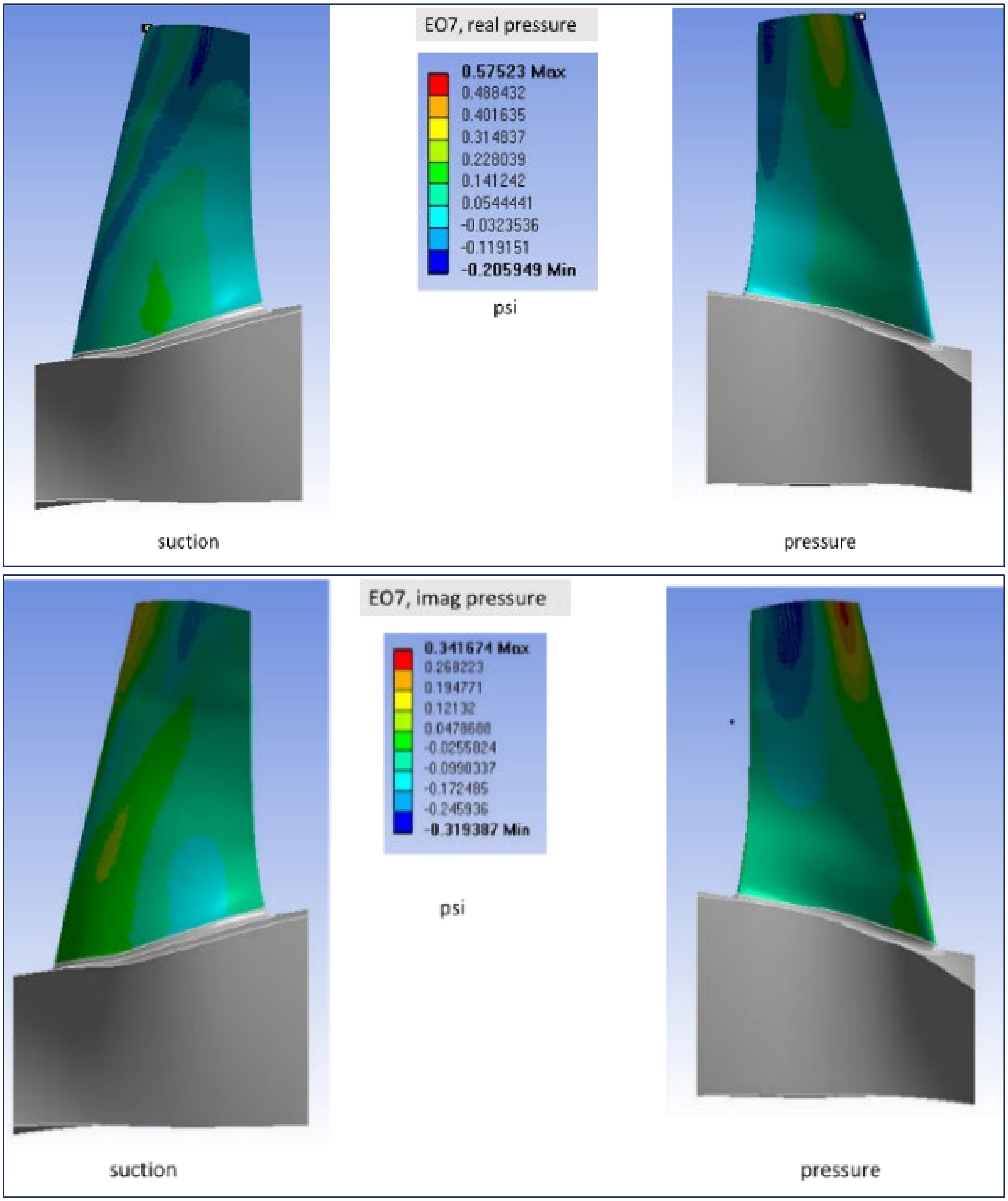

Figure 18.—Unsteady aerodynamic pressure contours (real and imaginary) for 7th EO harmonic excitation.

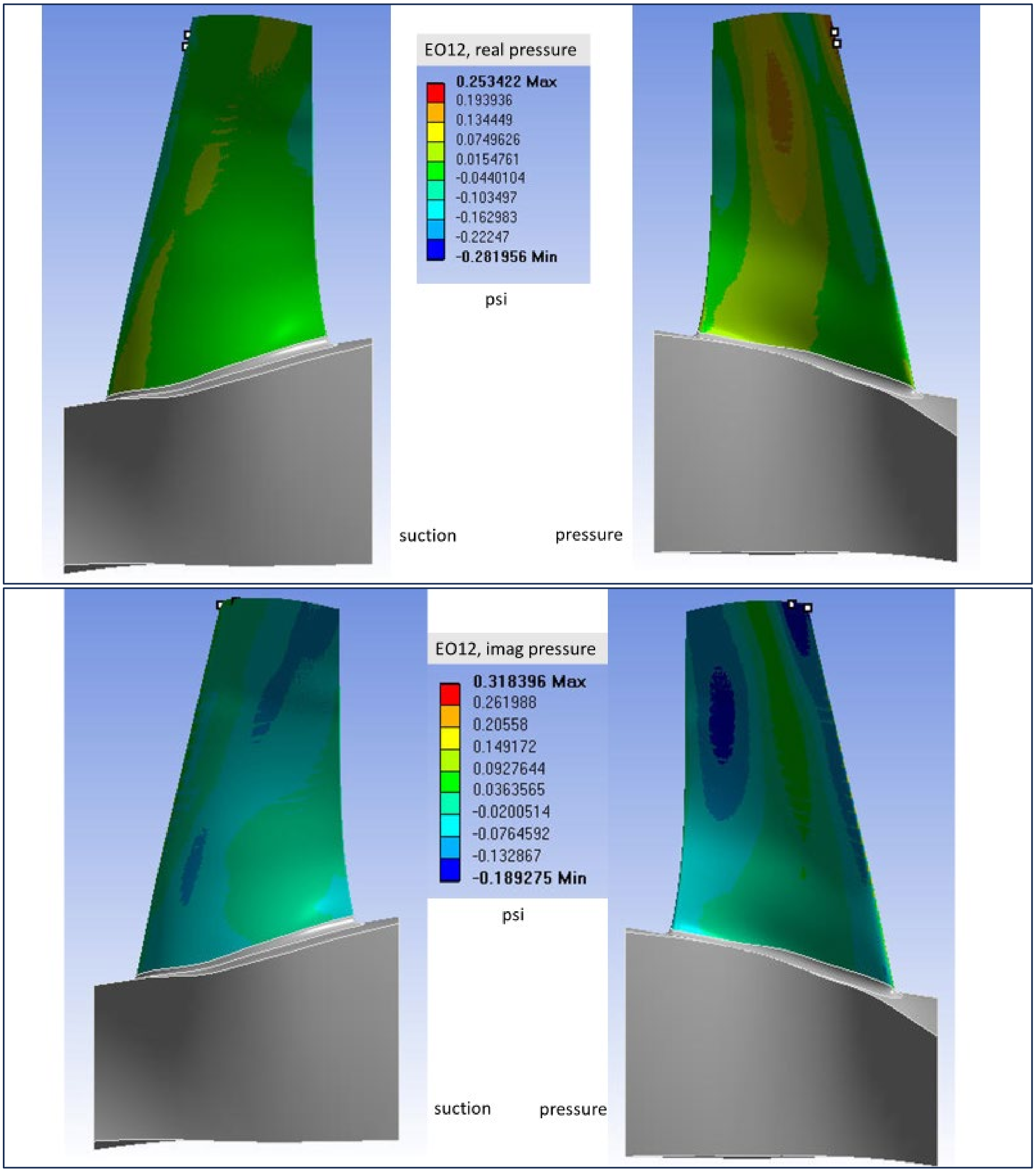

Figure 19.—Unsteady aerodynamic pressure contours (real and imaginary) for 12th EO harmonic excitation.

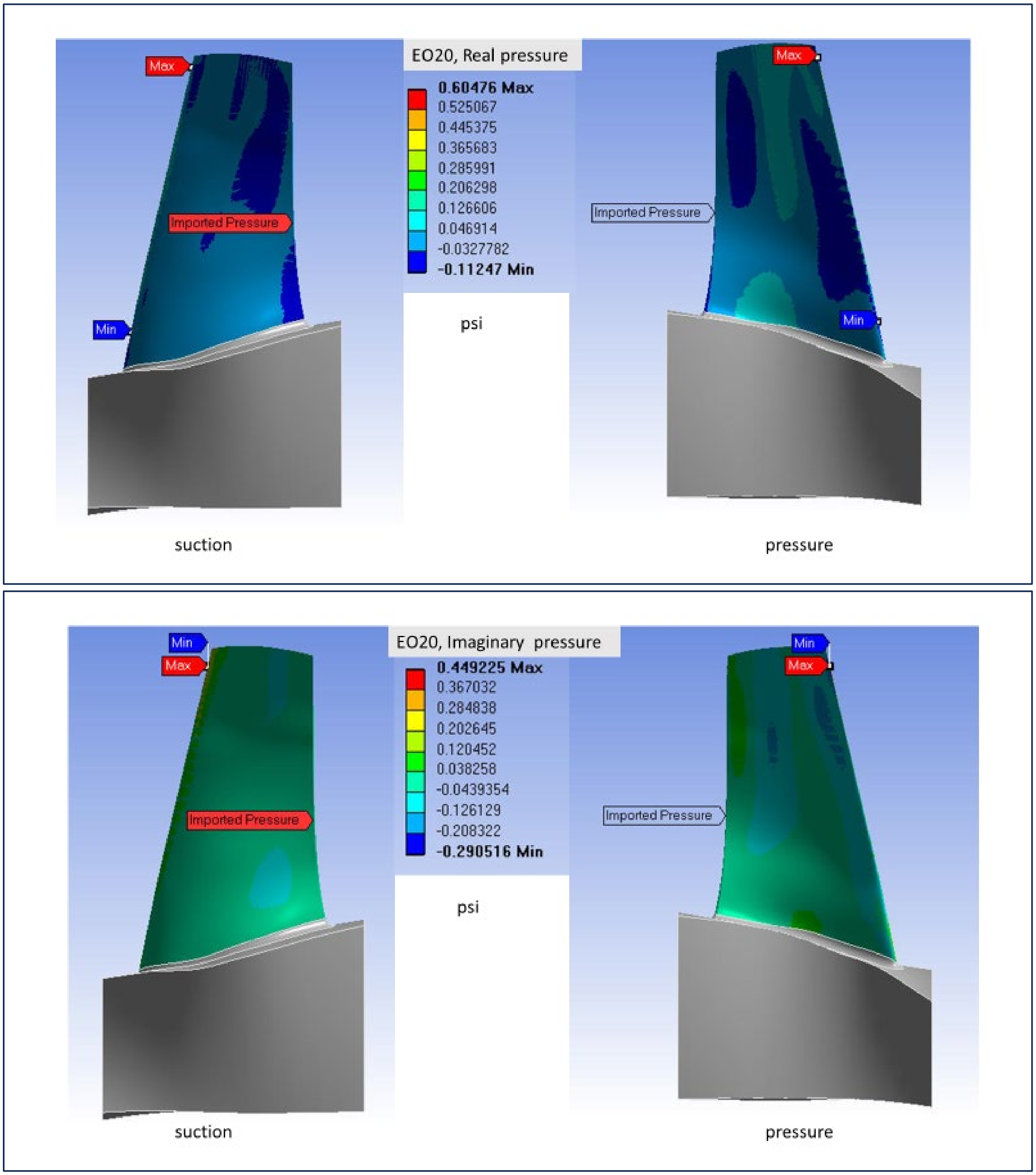

Figure 20.—Unsteady aerodynamic pressure contours (real and imaginary) for 20th EO harmonic excitation.

Forced response stress and displacement amplitudes, shown in Figure 21 to Figure 24, were numerically analyzed for modes associated with NDs of interest that align with EO excitations at the design speed (21,581 rpm). The analysis considered conditions that could potentially damage the blades due to near-resonance (crossing) effects, except for EO1, EO2, and EO3, as identified from the Campbell and interference diagrams. Note that the lower EOs (EO1 to EO3) are typically stronger excitation sources and are therefore included in the analysis, as shown in Figure 14, even though their frequency margins from the nearest mode are substantial.

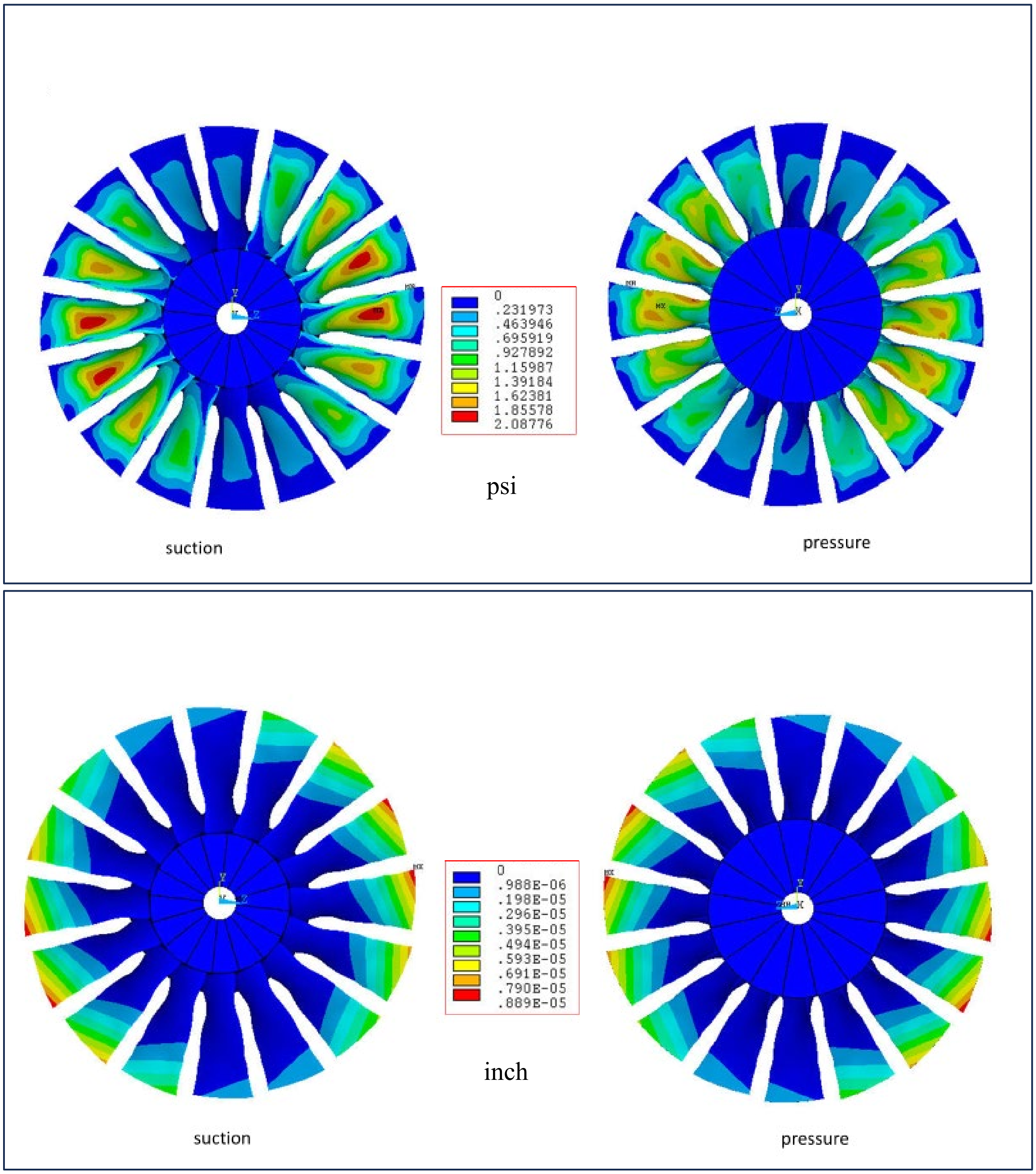

Figure 21.—Forced response dynamic stress contours (top) and displacement contours (bottom) for EO1 (360 Hz).

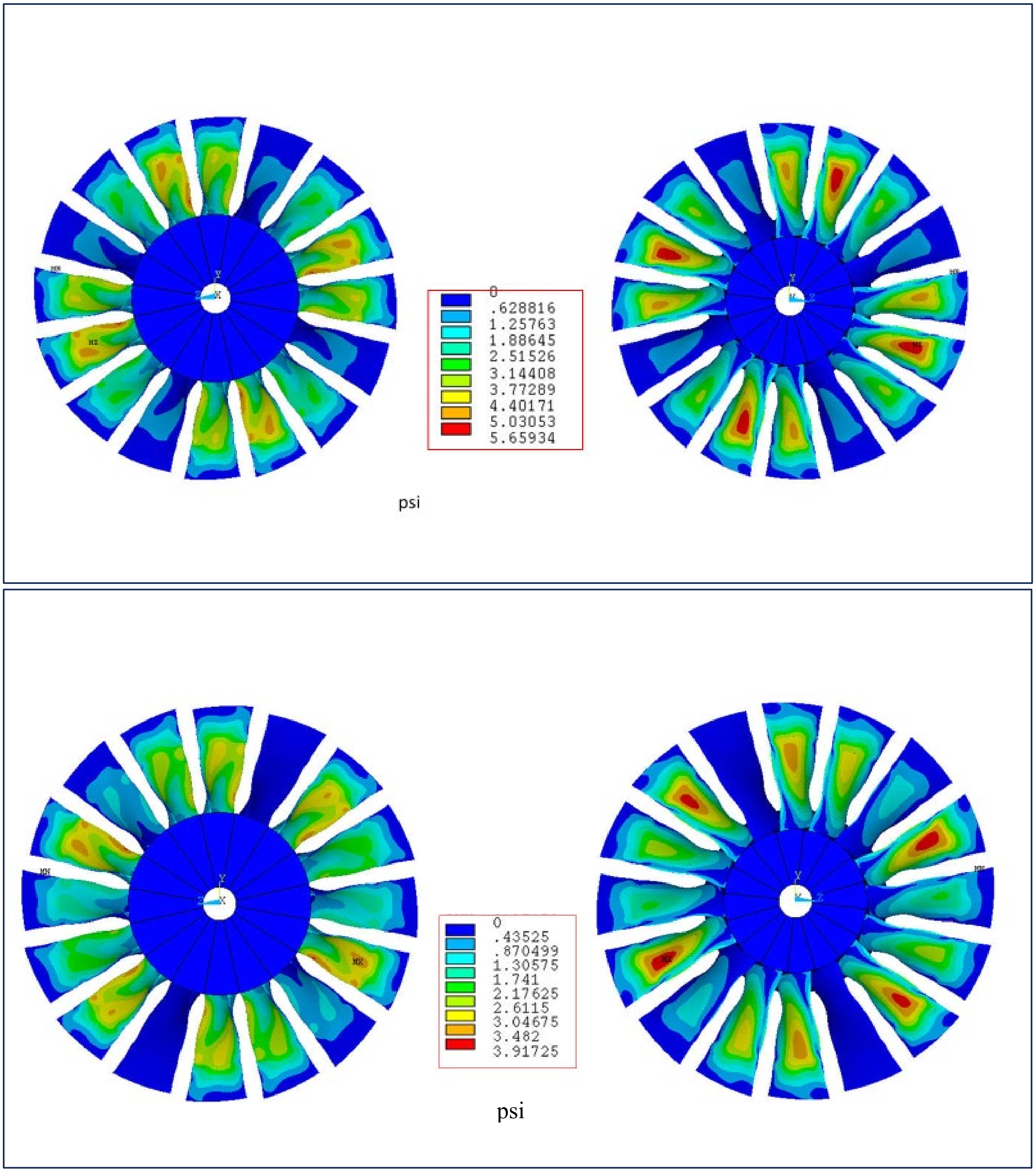

Figure 22.—Forced response dynamic stress contours for EO2 (720 Hz, top) and EO3 (1,079 Hz, bottom).

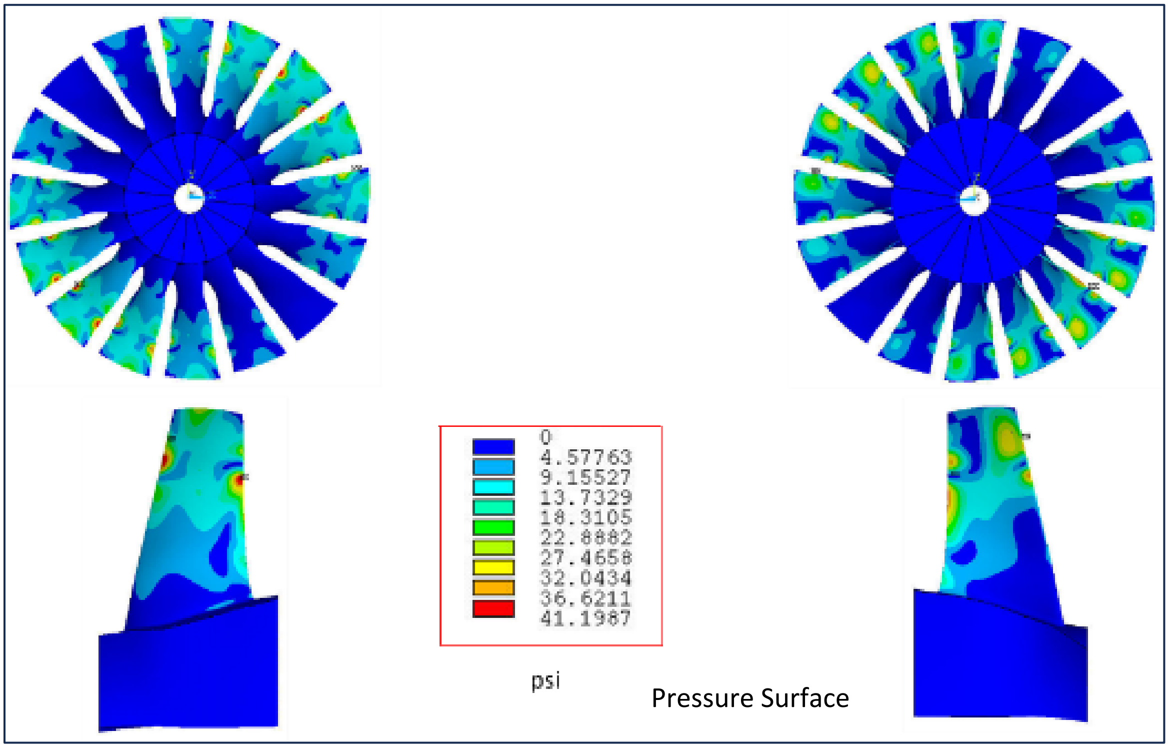

Figure 23.—Forced response dynamic stress contours for EO7 (2,518 Hz).

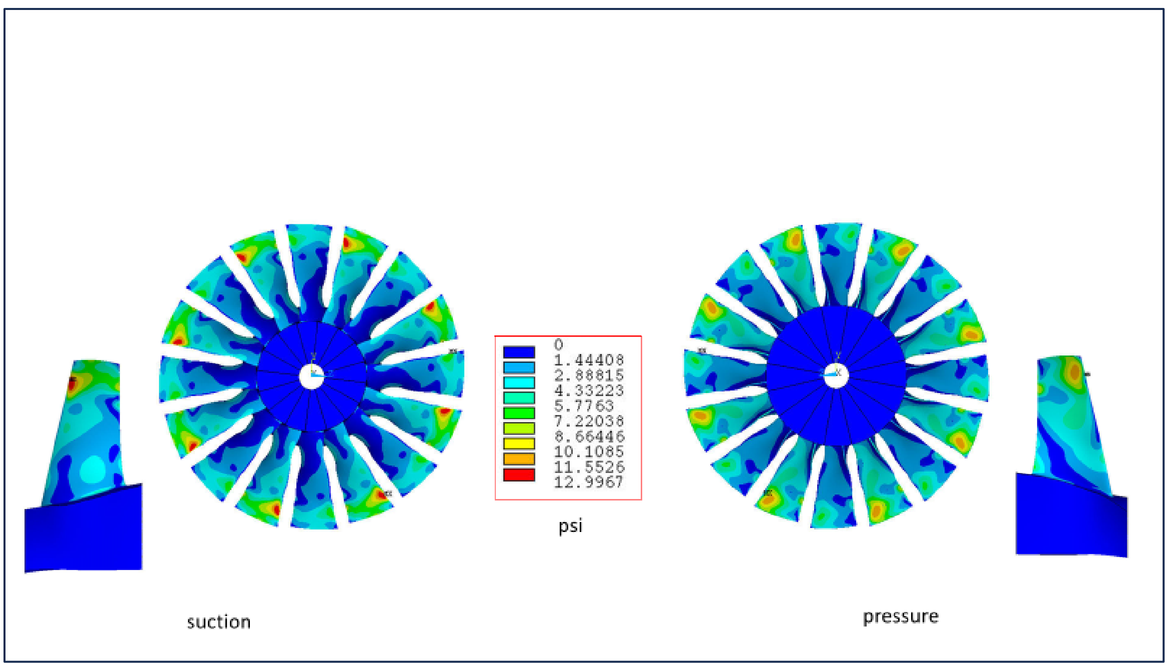

Figure 24.—Forced response dynamic stress contours for EO12 (4,316 Hz).

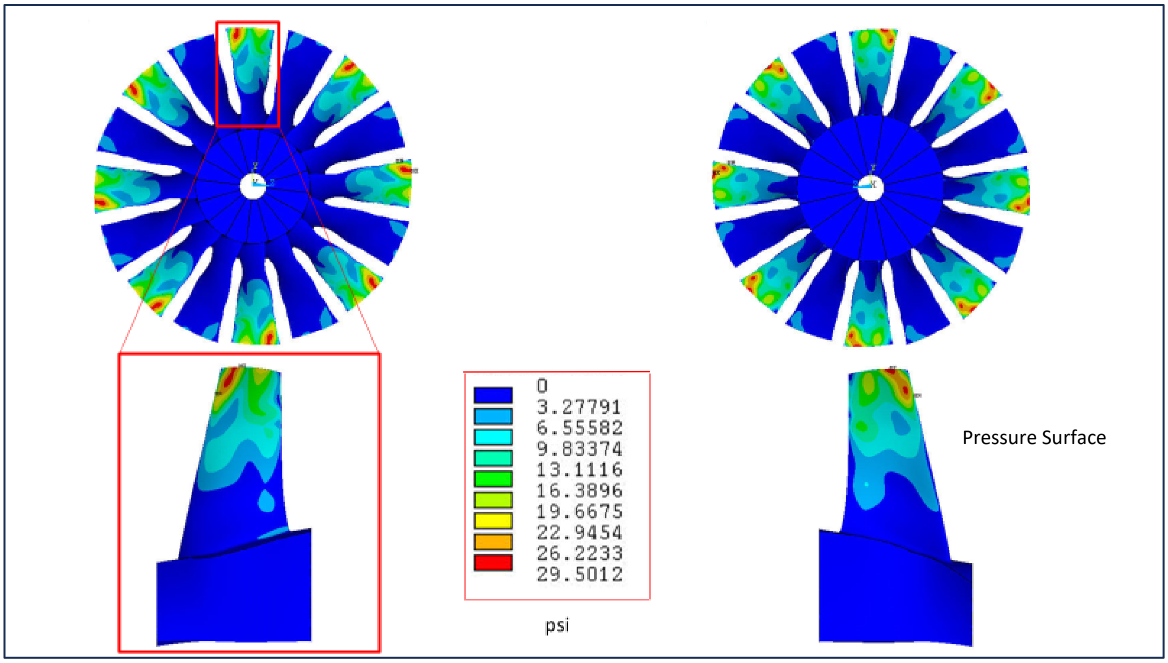

Figure 25.—Forced response dynamic stress contours for EO20 (7,194 Hz).

Next, a more detailed study of the forced response stress amplitudes associated with EO excitations of interest was conducted by examining the stress data at all nodes across the entire 16-blade TCT BLI DTF rotor model. Although the stress distribution at any given moment appears localized in certain blades due to the rotating wave nature of the excitation (as shown in Figure 25), the tuned nature of the rotor ensures that, over time, all blades experience the same dynamic stress amplitudes. This analysis helps confirm the uniformity of stress loading in a tuned system and provides insights into the overall structural behavior and potential failure mechanisms within the rotor.

The combined EO responses at the design speed—corresponding to the modes and NDs of interest identified from the Campbell diagram in Figure 14—were calculated. As shown in Figure 26, the numerical modeling results for the current TCT BLI DTF fan configuration indicate sufficient safety margins under design conditions. A Goodman diagram, also presented in Figure 26, was used to evaluate these safety margins based on the combined EO responses at the design speed. The diagram presents stress values for each FE node in the blade model, accurately representing their physical locations. Alternating stresses from various EO excitations were superimposed at each node to reflect the true combined effects, rather than simply summing the peak values from individual EOs—which typically occur at different locations on the blade. The primary objective of this cyclic symmetry forced response analysis was to assess whether the cumulative stress state at any location in the blade could pose a fatigue life concern for the current DTF blade configuration. It should be noted that, due to the proprietary nature of the original material limit data, an alternative material limit curve is used in the figure for illustrative purposes only.

The stress state at each node falls below the material limit line, indicating that the design meets the fatigue life requirement, with blade dynamic stress amplitudes remaining well below the allowable limit. According to established design criteria for compressors and turbines (Ref. 12), the mean stress in the TCT BLI DTF fan design satisfies the required yield design factor of 1.1. However, it does not meet the ultimate design factor of 1.5, which is necessary to ensure structural integrity under flight-representative structural testing conditions.

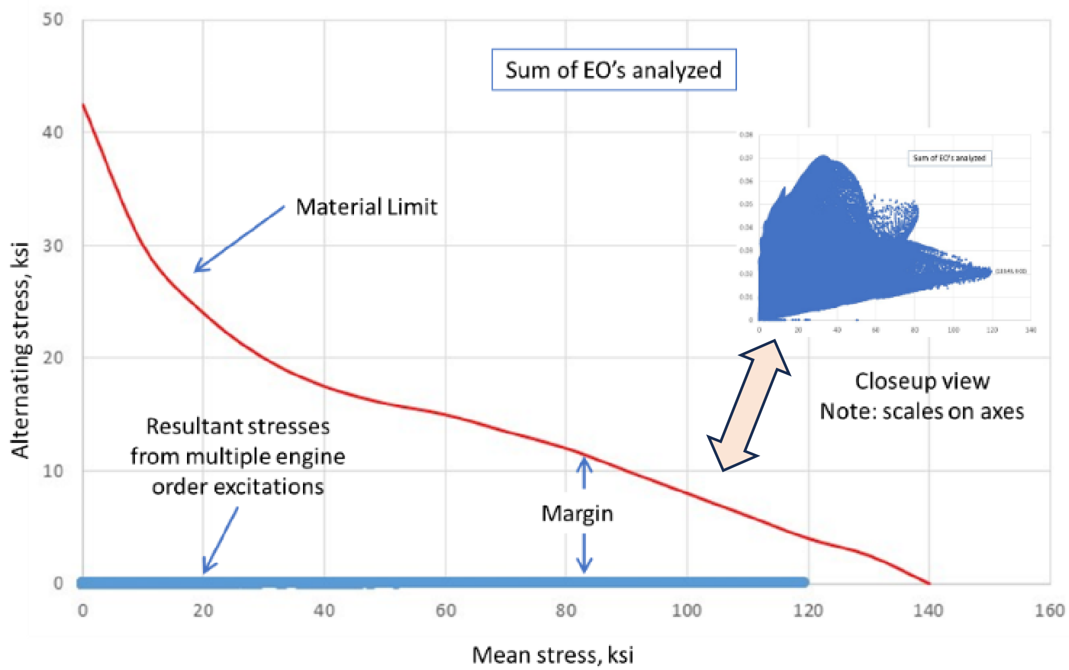

Figure 26.—Modified Goodman diagram incorporating data from TCT rotor model.

4.0 Concluding Remarks

A forced response assessment of the tail-cone thruster (TCT) boundary-layer ingestion (BLI) Distortion-Tolerant Fan (DTF) design configuration was conducted using finite element modeling (FEM) techniques, providing valuable insights into high cycle fatigue risks and the potential for engine failure due to boundary-layer distortion ingested by the TCT fan. Based on numerical results under the TCT BLI DTF design conditions, the fan blade configuration demonstrates acceptable safety margins. To increase confidence in the analysis, experimental validation through wind tunnel testing is recommended.

Although dynamic stresses are predicted to be relatively low, the high mean stress raises concerns about the available fatigue margin, as seen in the Goodman diagram. Several factors contribute to uncertainty in the analysis: blade-to-blade structural variations (mistuning) that can amplify dynamic response in localized blades, potential deviations in unsteady aerodynamic loading due to computational fluid dynamics (CFD) modeling limitations, and uncertainty in aerodynamic damping, which could elevate vibration amplitudes. If future high-fidelity CFD-based flutter or damping analyses are available, this damping estimate could be refined, potentially allowing for optimized structural design with improved confidence in vibration margins.

Given these uncertainties, the limited fatigue margin in the current design highlights the importance of using the analysis as a guiding tool—supplemented by physical testing to validate results and monitor stress levels to ensure material limits are not exceeded. The design load should encompass all relevant load cases and cycles throughout the service life, including self-induced conditions arising during operation.

Despite these challenges, this study establishes a solid framework for high-fidelity forced response analysis. Future improvements should focus on incorporating refinements that reduce key sources of uncertainty, thereby strengthening confidence in structural assessments and guiding design evolution.

References

1. https://www1.grc.nasa.gov/aeronautics/eap/airplane-concepts/starc-abl
2. Ralph H. Jansen, Cheryl Bowman, Amy Jankovsky, Rodger Dyson, James Felder: Overview of NASA Electrified Aircraft Propulsion Research for Large Subsonic Transports, AIAA-2017-4701.
3. Yehia El-Aini, Robert deLaneuville, Alan Stoner, Vincent Capece: High cycle fatigue of turbomachinery components - Industry perspective, AIAA Paper No. 97-3365, 33rd Joint Propulsion Conference and Exhibit, 1997.
4. J.B. Min, T.S.R. Reddy, M.A. Bakhle, et al: Cyclic Symmetry Finite Element Forced Response Analysis of a Distortion-Tolerant Fan with Boundary Layer Ingestion, 2018 AIAA Aerospace Sciences Meeting, AIAA SciTech Forum, Paper 2018-1890, 8–12 January 2018, Kissimmee, Florida.
5. Chen, J.-P., Briley, W. R.: A Parallel Flow Solver for Unsteady Multiple Blade Row Turbomachinery Simulations, ASME Paper GT2001-0348, June 2001.
6. Srivastava, R., Bakhle, M. A., Keith, T. G., Jr.: Numerical Simulation of Aerodynamic Damping for Flutter Analysis of Turbomachinery Blade Rows, AIAA Journal of Propulsion and Power, vol. 19, no. 2, March 2003.
7. Dickens, John M.: Numerical Methods for Dynamic Substructure Analysis, Ph.D. Thesis, University of California, Berkeley, 1980.
8. E.L. Wilson, E.P. Bayo, J.M. Dickens: Use of Special Ritz Vectors in Dynamic Substructure Analysis, Journal of Structural Engineering, ASCE, Volume 112, Issue 8, August 1986.
9. D.L. Thomas: Dynamics of rotationally periodic structures. International Journal for Numerical Methods in Engineering, 1979, 14 (1), pp. 81–102.
10. Cook, R.D., Malkus, D.S., Plesha, M.E., & Witt, R.J. (2002). *Concepts and Applications of Finite Element Analysis* (4th ed.). Wiley.
11. Klaus-Jurgen Bathe. *Finite Element Procedures in Engineering Analysis*, Prentice-Hall, 1982.
12. Rotating Machinery Design Guide, Section 1.18, Engineering Directorate, Internal Document, NASA Lewis Research Center (now NASA Glenn Research Center).